THE JOURNAL OF BIOLOGICAL CHEMISTRY VOL. 286, NO. 51, pp. 43855–43870, December 23, 2011

Lipocalin-2 Is a Chemokine Inducer in the Central Nervous System

ROLE OF CHEMOKINE LIGAND 10 (CXCL10) IN LIPOCALIN-2-INDUCED CELL MIGRATION[*S]

Received for publication, August 31, 2011, and in revised form, October 20, 2011 Published, JBC Papers in Press, October 26, 2011, DOI 10.1074/jbc.M111.299248

Shinrye Lee[‡], Jong-Heon Kim[‡], Jae-Hong Kim[‡], Jung-Wan Seo[‡], Hyung-Soo Han[§], Won-Ha Lee[¶], Kiyoshi Mori[‖], Kazuwa Nakao[‖], Jonathan Barasch[**], and Kyoungho Suk[‡1]

*From the Departments of [‡]Pharmacology and [§]Physiology, Brain Science & Engineering Institute, Cell and Matrix Research Institute, and the [¶]School of Life Sciences and Biotechnology, Kyungpook National University School of Medicine, Daegu 700-422, Korea, the [‖]Department of Medicine and Clinical Science, Kyoto University Graduate School of Medicine, Kyoto 606-8507, Japan, and the **Department of Medicine, College of Physicians and Surgeons, Columbia University, New York, New York 10027*

Background: LCN2 has been implicated in cell morphology and migration.
Results: LCN2 promotes cell migration through up-regulation of chemokines (CXCL10) in brain both *in vitro* and *in vivo*.
Conclusion: LCN2 is a chemokine inducer in the CNS and may accelerate cell migration under inflammatory conditions in an autocrine or paracrine manner.
Significance: LCN2 could be targeted to therapeutically modulate glial responses in various neuroinflammatory disease conditions.

The secreted protein lipocalin-2 (LCN2) has been implicated in diverse cellular processes, including cell morphology and migration. Little is known, however, about the role of LCN2 in the CNS. Here, we show that LCN2 promotes cell migration through up-regulation of chemokines in brain. Studies using cultured glial cells, microvascular endothelial cells, and neuronal cells suggest that LCN2 may act as a chemokine inducer on the multiple cell types in the CNS. In particular, up-regulation of CXCL10 by JAK2/STAT3 and IKK/NF-κB pathways in astrocytes played a pivotal role in LCN2-induced cell migration. The cell migration-promoting activity of LCN2 in the CNS was verified *in vivo* using mouse models. The expression of LCN2 was notably increased in brain following LPS injection or focal injury. Mice lacking LCN2 showed the impaired migration of astrocytes to injury sites with a reduced CXCL10 expression in the neuroinflammation or injury models. Thus, the LCN2 proteins, secreted under inflammatory conditions, may amplify neuroinflammation by inducing CNS cells to secrete chemokines such as CXCL10, which recruit additional inflammatory cells.

Lipocalin 2 (LCN2)[2] is a small hydrophobic molecule-binding protein that is also called 24p3. LCN2 plays an important role in diverse cellular processes, such as cell death/survival (1–4), cell migration/invasion (5, 6), cell differentiation (7, 8), iron delivery (1, 7, 9, 10), inflammation (11), and insulin resistance (12). There is, however, a debate on the role of LCN2 in cell migration. Previously, LCN2 facilitated gastrointestinal mucosal regeneration by promoting cell migration (13). Recently, LCN2 was also associated with an increased cytokine secretion and migratory activity of endometrial cancer (14). In ovarian cancer, however, LCN2 expression blocked epithelial to mesenchymal transition, one of the hallmarks of invasive neoplasia (15). LCN2 reduced adhesion/invasion partly by suppressing FAK activation in pancreas carcinoma cells (16). In contrast to numerous publications on LCN2 in various peripheral tissues, little is known about the role of LCN2 in the CNS. Recently, we have reported that the LCN2 protein is secreted by microglia and astrocytes in the CNS and promotes morphological changes and cell migration in an autocrine manner (17, 18). However, it is not clearly understood how LCN2 induces reactive astrocytosis or how LCN2 orchestrates cell migration.

In the CNS, chemokines are generally found under both physiological and pathological conditions, such as development, synaptic transmission, homeostasis, injury, and disease-associated neuroinflammation (19–21). CNS chemokines can be classified, according to their function, into neuromodulatory and inflammatory chemokines. Neuromodulatory chemokines have a neurotransmitter/neuromodulatory role in the brain, with characteristics such as neuronal expression, colocalization with classical or peptide neurotransmitters, pre- and post-synaptic receptor localization, and electrophysiological effects (22). Chemokine (C*X*C motif) ligand 12 (CXCL12)/SDF-1, chemokine (CX_3C motif) ligand 1/fractalkine, and chemokine (C*X*C motif) ligand 1 (CXCL1)/GROα are a few examples of neuromodulatory chemokines. The major role of inflammatory

* This work was supported by National Research Foundation Grant 2009-0078941 funded by the Ministry of Education, Science and Technology of Korean government. This work was also supported by the Basic Science Research Program through the National Research Foundation funded by Ministry of Education, Science and Technology Grant 2010-0029460.
[S] The on-line version of this article (available at http://www.jbc.org) contains supplemental Figs. S1–S3.
[1] To whom correspondence should be addressed: Dept. of Pharmacology, Kyungpook National University School of Medicine, 101 Dong-In, Joong-gu, Daegu 700-422, Korea. Tel.: 82-53-420-4835; Fax: 82-53-256-1566; E-mail: ksuk@knu.ac.kr.
[2] The abbreviations used are: LCN2, lipocalin 2; CXCL, chemokine (C*X*C motif) ligand; ACM, astrocyte-conditioned medium; GFAP, glial fibrillary acidic protein; PIAS3, protein inhibitor of activated STAT3; CCL, chemokine (CC motif) ligand; dpi, days post-injury; icv, intracerebroventricular.

chemokines is the recruitment of effector cells to inflammation sites (23). The various types of inflammatory chemokines include chemokine (CC motif) ligand 2 (CCL2)/MCP-1, chemokine (CC motif) ligand 5 (CCL5)/RANTES, chemokine (C*X*C motif) ligand 2 (CXCL2)/IL-8, and chemokine (C*X*C motif) ligand 10 (CXCL10)/IP-10. CXCL10, which is also known as IP-10 (IFN-γ-inducible protein of 10 kDa) (24, 25), acts via the CXCR3 receptor and is expressed in both glia and neuronal cells in the CNS (26, 27). The expression of CXCL10 is often triggered by inflammatory mediators, such as LPS (28), IFN-γ (24), or microbial toxins (29). Increased CXCL10 levels were considered to be critical for the increased migration of inflammatory cells into the CNS (30, 31). Many different CNS cells have been identified as sources of chemokines, including microglia, astrocytes, neuronal cells, and endothelial cells (27, 32). However, the existence of regulatory mechanisms of inflammatory chemokine expression in the brain is far from clear.

In the present study, we present evidence that LCN2 up-regulates chemokine expression in multiple cell types in the CNS, thereby providing a molecular basis of LCN2-induced cell migration that has been previously observed in the CNS, as well as peripheral tissues. In particular, astrocyte-derived CXCL10 plays a central role in LCN2-induced cell migration. Additionally, our results indicate that JAK2/STAT3 and NF-κB pathways partly mediate LCN2 up-regulation of CXCL10 and glial fibrillary acidic protein (GFAP) expression in astrocytes. Using mouse model, we confirmed that LCN2 influences CNS cell migration *in vivo*. Our results revealed a strong induction of LCN2 in the mouse brain following LPS injection or injury. Notably, there was a pronounced reduction in astrocyte migration and GFAP/CXCL10 expression in brain of LCN2-deficient ($LCN2^{-/-}$) mice. The *in vitro* and *in vivo* data point to a key role for LCN2-CXCL10 axis in cell migration and reactive astrocytosis following brain inflammation or injury.

EXPERIMENTAL PROCEDURES

Reagents and Cells—The following chemicals were obtained from Sigma: LPS from *Escherichia coli* 0111:B4 prepared by phenolic extraction and gel filtration chromatography, phorbol 12-myristate 13-acetate, ATP, pyrrolidine dithiocarbamate, and polymyxin B. JAK2 inhibitor ((*E*)-*N*-benzyl-2-cyano-3-(3,4-dihydroxyphenyl)acrylamide α-cyano-(3,4-dihydroxy)-*N*-benzylcinnamide tyrphostin B42; AG490), JAK1 inhibitor (*trans*-3,3′,4,5′-tetrahydroxystilbene; piceatannol), and IKK-2 inhibitor (SC-514) were purchased from Calbiochem (La Jolla, CA). The recombinant human TNF-α, mouse IFN-γ, and NSO murine melanoma cell-derived mouse LCN2 proteins were purchased from R & D Systems (Minneapolis, MN). The bacterially expressed recombinant mouse LCN2 protein was prepared, as previously described (18). In brief, the recombinant mouse LCN2 protein was expressed as a GST fusion protein in the BL21 strain of *E. coli*, which does not synthesize siderophore. The protein was purified by using glutathione-Sepharose 4B beads (GE Healthcare). All other chemicals, unless otherwise stated, were obtained from Sigma. The transformed mouse cerebral endothelial cell line, bEnd.3 (CRL-2299; ATCC, Manassas, VA) (33), was grown in DMEM supplemented with 10% FBS (Invitrogen), 100 units/ml penicillin, and 100 μg/ml streptomycin (Invitrogen). C6 rat glioma cells were maintained in DMEM supplemented with 5% heat-inactivated FBS (Invitrogen) and gentamicin (50 μg/ml). The mouse primary astrocyte and microglia cultures were prepared from the brains of 0–3-day-old ICR mice (Samtako Co., Osan, Korea), as previously described (18). The purity levels of astrocyte and microglia cultures were >96% and >95% as determined by GFAP and isolectin B4 staining, respectively. Primary cultures of dissociated cerebral cortical neurons were prepared from embryonic day 20 ICR mice, as described previously (34, 35). Briefly, mouse embryos were decapitated, and the brains were rapidly removed and placed in a culture dish with cold PBS. The cortices were isolated and then transferred to a culture dish containing 0.25% trypsin-EDTA (Invitrogen) in PBS for 30 min at 37 °C. After two washes in serum-free neurobasal medium (Invitrogen), the cortical tissues were mechanically dissociated with a gentle pipetting. Dissociated cortical cells were seeded onto 6-well plates coated with poly-D-lysine (Falcon; BD Biosciences), using neurobasal medium containing 10% FBS, 0.5 mM glutamine, 100 units/ml penicillin, 100 μg/ml streptomycin, N2 supplement (Invitrogen), and a B27 supplement (Invitrogen). The cells were maintained by changing the media every 2–3 days and were grown at 37 °C in a 5% CO_2 humidified atmosphere. The purity of the neuronal cultures was determined by immunocytochemical staining, using an antibody against a neuron-specific marker, microtubule-associated protein 2 (Promega, Madison, WI). Animals used in the current research were acquired and cared for in accordance with guidelines published in the National Institutes of Health Guide for the Care and Use of Laboratory Animals. The study was approved by the institutional review board of the Kyungpook National University School of Medicine.

DNA Microarray Analysis—Mouse primary astrocyte cultures were treated with the recombinant LCN2 protein (10 μg/ml) or left untreated for 8 h. Total RNA was isolated and labeled with either cyanine 3- or cyanine 5-conjugated dCTP (Amersham Biosciences) by a reverse transcription reaction, using reverse transcriptase SuperScript II (Invitrogen). The labeled cDNAs were mixed, placed on an Agilent mouse whole oligonucleotide chip (G4122A; Agilent Technologies, Santa Clara, CA), and covered by a hybridization chamber. Hybridized slides were scanned with the Axon Instruments GenePix 4000B scanner, and the scanned images were analyzed with the software programs GenePix Pro 5.1 (Axon, Union City, CA) and GeneSpring 7.2 (Sillicongenetics, Redwood City, CA). A complete description of the DNA microarray platform and results is available under Gene Expression Omnibus accession number GSE15667.

Traditional Reverse Transcription-PCR and Real Time PCR—Total RNA was extracted from cells and adult mouse tissues by using the TRIzol reagent (Invitrogen), according to the manufacturer's protocol. Reverse transcription was conducted using Superscript II (Invitrogen) and oligo(dT) primer. PCR amplification, using specific primer sets, was carried out at a 55–60 °C annealing temperature for 20–30 cycles. The PCR was performed by using a DNA Engine Tetrad Peltier Thermal Cycler (MJ Research, Waltham, MA). For the analysis of PCR products, 10 μl

TABLE 1
DNA sequences of the primers used for traditional and real time RT-PCR

Mouse cDNAs	RT-PCR type	Primer sequences	GenBank™ accession number	Amplicon size
				bp
ccl4	Traditional	Forward, 5′-GCC CTC TCT CTC CTC TTG CT-3′ Reverse, 5′-GTC TGC CTC TTT TGG TCA GG-3′	NM_013652	196
ccl20	Traditional	Forward, 5′-CGA CTG TTG CCT CTC GTA CA-3′ Reverse, 5′-AGG AGG TTC ACA GCC CTT TT-3′	NM_016960	177
cxcl2	Traditional	Forward, 5′-AGT GAA CTG CGC TGT CAA TG-3′ Reverse, 5′-TTC AGG GTC AAG GCA AAC TT-3′	NM_009140	303
cxcl10	Traditional and real time	Forward, 5′-AAG TGC TGC CGT CAT TTT CT-3′ Reverse, 5′-GTG GCA ATG ATC TCA ACA CG-3′	NM_021274	186
il-6	Traditional and real time	Forward, 5′-AGT TGC CTT CTT GGG ACT GA-3′ Reverse, 5′-TCC ACG ATT TCC CAG AGA AC-3′	NM_031168	159
cox2	Traditional	Forward, 5′-GAA GGG ACA CCC TTT CAC AT-3′ Reverse, 5′-ACA CTC TAT CAC TGG CAT CC-3′	NM_011198	565
inos	Traditional	Forward, 5′-CCC TTC CGA AGT TTC TGG CAG CAG C-3′ Reverse, 5′-GGC TGT CAG AGC CTC GTG GCT TTG G-3′	NM_010927	497
inos	Real time	Forward, 5′-GCC ACC AAC AAT GGC AAC A-3′ Reverse, 5′-CGT ACC GGA TGA GCT GTG AAT T-3′	NM_010927	103
pias3	Traditional	Forward, 5′-GGA CGT GTC CTG TGT GTG AC-3′ Reverse, 5′-CTC TGA TGC CTC CTT CTT GG-3′	NM_018812	158
lcn2	Traditional and real time	Forward, 5′-ATG TCA CCT CCA TCC TGG TC-3′ Reverse, 5′-CAC ACT CAC CAC CCA TTC AG-3′	NM_008491	363
24p3R	Traditional	Forward, 5′-AAT GAC TCT CAC GGG GAT TG-3′ Reverse, 5′-AGT GGT GGG GAT GAC TTC AG-3′	NM_021551	157
megalin	Traditional	Forward, 5′-CCA GAA AAT GTG GAA AAC CAG-3′ Reverse, 5′-ACA AGG TTT GCG GTG TCT TT-3′	NM_001081088	308
cxcr3	Traditional	Forward, 5′-TGC CAG TAC AAC TTC CCA CA-3′ Reverse, 5′-TGC CAC CAC CAC TAC CAC TA-3′	NM_009910	180
gfap	Traditional and real time	Forward, 5′-AGG CAG AAG CTC CAA GAT GA-3′ Reverse, 5′-TGT GAG GTC TGC AAA CTT GG-3′	NM_010277	342
β-actin	Traditional	Forward, 5′-ATC CTG AAA GAC CTC TAT GC-3′ Reverse, 5′-AAC GCA GCT CAG TAA CAG TC-3′	NM_007393	287
gapdh	Real time	Forward, 5′-TGG GCT ACA CTG AGC ACC AG-3′ Reverse, 5′-GGG TGT CGC TGT TGA AGT CA-3′	NM_008084	171

of each PCR was electrophoresed on 1% agarose gel and detected under UV light. β-Actin was used as an internal control. The real time PCR was performed using one-step SYBR® PrimeScript™ RT-PCR kit (Perfect Real Time; Takara Bio Inc., Tokyo, Japan) according to the manufacturer's instructions, followed by detection using the ABI Prism® 7000 sequence detection system (Applied Biosystems, Foster City, CA). The $2^{-\Delta\Delta CT}$ method was used to calculate relative changes in gene expression determined by real time PCR experiments (36). Nucleotide sequences of the primers were based on published cDNA sequences (Table 1).

CXCL10 ELISA—The levels of CXCL10 in the culture media were measured by sandwich ELISA using a rat monoclonal anti-mouse CXCL10 antibody as the capture antibody and goat biotinylated polyclonal anti-mouse CXCL10 antibody as a detection antibody (ELISA development reagent; R & D Systems), respectively, as previously described (37). The recombinant mouse CXCL10 protein (R & D Systems) was used as a standard. The monoclonal anti-mouse CXCL10 antibody and the recombinant mouse CXCL10 protein were also used for cell migration assay.

Astrocyte-conditioned Media—To prepare astrocyte-conditioned medium (ACM), primary astrocytes prepared from the brains of 0–3-day-old ICR mice were cultured at the density of 1.5×10^6 cells in 100-mm plates in DMEM, supplemented with 10% FBS for 24 h. Primary astrocyte cultures were treated with the recombinant LCN2 protein (10 μg/ml) or left untreated for 24 h. The cells were then washed twice with PBS and cultured in fresh DMEM for an additional 24 h. The ACM was then collected, centrifuged at 1000 rpm for 5 min to remove cell debris, and stored at −80 °C until further analysis.

Cell Migration Assays—Cell migration was determined by using a 48-well Boyden chamber (NeuroProbe, Gaithersburg, MD), according to the manufacturer's instructions. ACM, the recombinant CXCL10 protein, or anti-CXCL10 antibody was placed into base wells separated from the top wells by polyvinylpyrrolidone-free polycarbonate filters (8-μm pore size; 25 × 80 mm; NeuroProbe). The cells were harvested by trypsinization, resuspended in DMEM, and added to the upper chamber at a density of 1×10^4 cells/well. The cells were incubated at 37 °C under 5% CO_2 for 12 to 72 h. Zigmond-Hirsch checkerboard analysis (38) was performed in triplicate to distinguish between concentration-dependent cell migration (chemotaxis) and random migration (chemokinesis). ACM and the recombinant CXCL10 protein of varying concentrations were added to the upper and/or lower wells of the Boyden chambers for the checkerboard analysis. For the checkerboard analysis, trypsinized cells were added to the upper chamber at a density of 2×10^4 cells/well and incubated for 48 h. At the end of the incubation, nonmigrating cells on the inner side of the membrane were removed with a cotton swab. Migrated cells on the underside of the membrane were fixed with methanol for 10 min and stained with Mayer's hematoxylin (Dakocytomation, Glostrup, Denmark) for 20 min. Photomicrographs of five randomly chosen fields were taken (Olympus CK2, Tokyo, Japan) (original magnification, ×100), and the cells were enumerated to calculate the average number of cells that had migrated. All of the migrated cells were counted, and the results were presented as the means ± S.D. of triplicate results. The *in vitro* scratch wound healing assay was performed as previously described (39). In brief, a scratch wound was created by using a

TABLE 2

Partial list of genes that were up or down-regulated by LCN2 as determined by DNA microarray analysis of astrocytes

Genes whose expression was increased or decreased greater than 1.5- or 3.5-fold, respectively, by LCN2 were listed.

Description	Gene symbol	GenBank™ accession number	Fold change
Increased expression			
Chemokine (CC motif) ligand 20	CCL20	NM_016960	6.50077
Immunoresponsive gene 1	IRG1	XM_127883	5.09345
Interleukin 6	IL-6	NM_031168	4.77762
Chemokine (CC motif) ligand 4	CCL4	NM_013652	3.90144
Chemokine (*C*XC motif) ligand 2	CXCL2	NM_009140	3.58657
Chemokine (*C*XC motif) ligand 1	CXCL1	NM_008176	3.55145
Nitric-oxide synthase 2, inducible, macrophage	Nos2	NM_010927	3.51580
Chemokine (CC motif) ligand 3	CCL3	NM_011337	3.28548
Chemokine (CC motif) ligand 5	CCL5	NM_013653	2.54231
Chemokine (*C*XC motif) ligand 5	CXCL5	NM_009141	2.40575
Chemokine (CC motif) ligand 7	CCL7	NM_013654	2.34586
Chemokine (*C*XC motif) ligand 10	CXCL10	NM_021274	2.19630
Chemokine (*C*XC motif) ligand 9	CXCL9	NM_008599	2.19380
Pentraxin-related gene	PTX3	NM_008987	2.05385
Prostaglandin-endoperoxide synthase 2	COX-2	NM_011198	1.95792
Toll-like receptor 2	TLR2	NM_011905	1.84527
Decreased expression			
Calumenin	CALU	NM_184053	0.21026
Expressed sequence AI597479	AI597479	NM_133818	0.23034
Protein inhibitor of activated STAT 3	PIAS3	NM_018812	0.23293
Nuclear receptor-binding protein	NRBP	NM_147201	0.23797
Cell cycle progression 1	CCPG1	NM_028181	0.24613
RAB31, member RAS oncogene family	RAB31	NM_133685	0.24669
Ubiquitin-conjugating enzyme E2G 2	UBE2G2	NM_019803	0.24804
TBC1 domain family, member 14	TBC1D14	NM_133910	0.25170
DEA(D/H) (Asp-Glu-Ala-(Asp/His)) box polypeptide 3, *X*-linked	DDX3X	NM_010028	0.25526
Eukaryotic translation elongation factor 2	EEF2	NM_007907	0.26471
Rho guanine nucleotide exchange factor 10	ARHGEF10	NM_172751	0.26643
Solute carrier family 25 (mitochondrial carrier, phosphate carrier), member 25	SLC25A25	NM_146118	0.26660
Zinc finger, UBR1 type 1	ZUBR1	XM_001479455	0.26705
Similar to RAN-binding protein 5	LOC436227	XM_621068	0.26737
Guanine nucleotide binding protein, α12	GNA12	NM_010302	0.26968
Ets variant gene 5	ETV5	NM_023794	0.27306
AFG3 (ATPase family gene 3)-like 2 (yeast)	AFG3L2	NM_027130	0.27435
HECT, UBA, and WWE domain-containing 1	HUWE1	NM_021523	0.27821
Cytoplasmic linker 2	CYLN2	NM_009990	0.27926

10-μl pipette tip on confluent cell monolayers in 24-well culture plates and placed into DMEM containing 10% FBS, 100 units/ml penicillin, and 100 μg/ml streptomycin. The cells were incubated at 37 °C under 5% CO_2 during migration of monolayer into the cleared wound area. The wound area was observed by microscopy (Olympus CK2) (magnification, $\times$100). Relative cell migration distance was determined by measuring the wound width and subtracting this from the initial value as previously described: cell migration distance = initial wound width at day 0 − wound width at the day of measurement (40). Three nonoverlapping fields were selected and examined in each well (three wells/experimental group). The results were presented as a fold increase of migration distance.

Morphological Analysis of Astrocytes, Microglia, and Neuron Cells—The morphological analysis of astrocytes or neuron cells was performed by using fluorescence microscopy (Olympus BX50). The cells were blocked with 1% BSA in PBS-Tween 20 for 10 min and incubated in PBS containing 3% BSA and mouse anti-GFAP antibody (1:30 dilution; Biogenex, San Ramon, CA) or mouse anti-microtubule-associated protein 2 antibody (1:600 dilution; Promega). After two washes in PBS-Tween 20, the cells were incubated with anti-mouse IgG-FITC-conjugated secondary antibody (BD Biosciences). Astrocyte processes were quantified as previously described, but with a slight modification (18, 41, 42). The average process length was based on the longest process for each cell from a minimum of five randomly chosen microscopic fields containing at least 100 cells. Neuronal processes were quantified as previously described, but with a slight modification (43). In brief, the total number of neuronal processes longer than one cell body diameter was counted. The number of neuronal processes was determined from a minimum of five randomly chosen microscopic fields containing at least 100 cells. The morphological analysis of microglia was performed by using phase contrast microscopy following peroxidase-labeled isolectin B4 staining (1:500 dilution; Sigma) (17). Deramification of microglia was quantified as previously described with a slight modification (17, 44). The percentage of ramified cells was determined from a minimum of five randomly chosen fields containing at least 100 cells.

Western Blot Analysis—Astrocyte cultures or adult mouse tissues were lysed in triple-detergent lysis buffer (50 mM Tris-HCl, pH 8.0, 150 mM NaCl, 0.02% sodium azide, 0.1% SDS, 1% Nonidet P-40, 0.5% sodium deoxycholate, and 1 mM phenylmethylsulfonyl fluoride). Protein concentration in cell lysates was determined by using a Bio-Rad protein assay kit. An equal amount of protein from each sample was separated by 12% SDS-PAGE and transferred to Hybond ECL nitrocellulose membranes (Amersham Biosciences). The membranes were blocked with 5% skim milk and sequentially incubated with primary antibodies (rabbit polyclonal anti-phospho-STAT3 at Ser^{727}/Tyr^{705} and anti-total STAT3 antibodies (Cell Signaling Technology, Beverly, MA); mouse monoclonal anti-GFAP antibody (Biogenex); goat polyclonal anti-mouse LCN2 antibody (R & D Systems); and monoclonal anti-α-tubulin clone B-5–

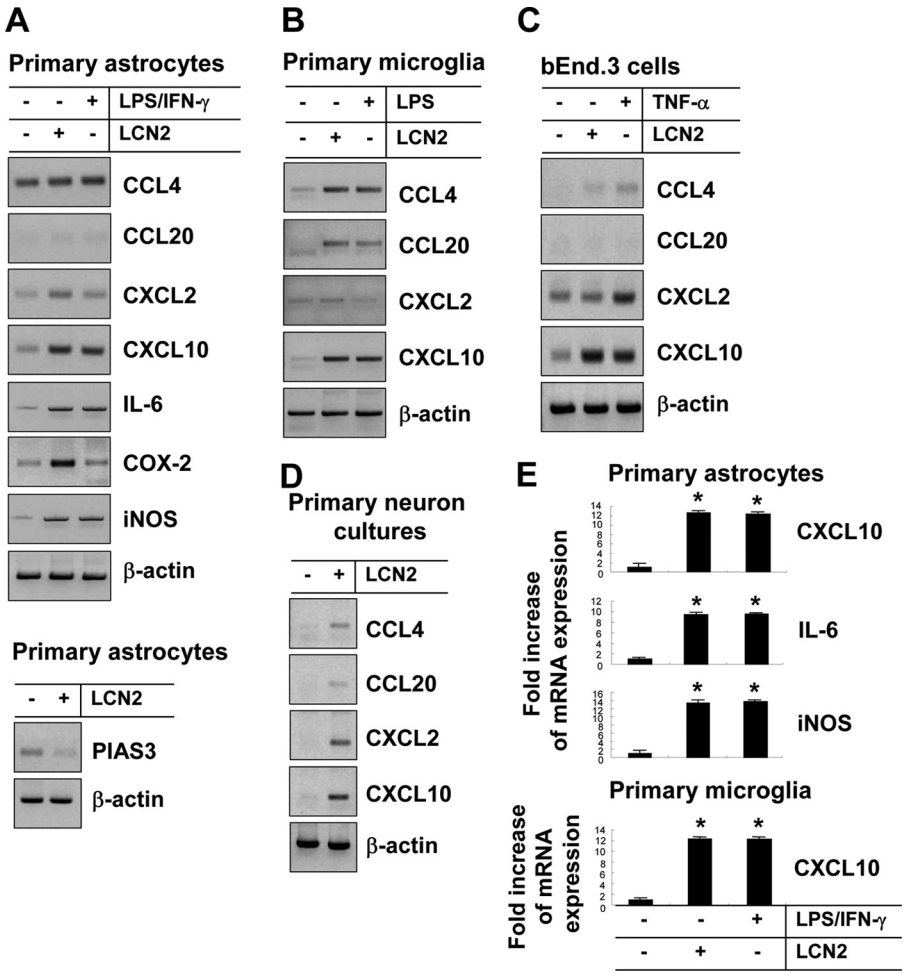

FIGURE 1. **Induction of chemokine gene expression by LCN2 in astrocytes, microglia, endothelial cells, and neuron cells.** Astrocytes (*A* and *E*), microglia (*B* and *E*), bEnd.3 endothelial cells (*C*), and neuron cells (*D*) were treated with the recombinant LCN2 protein (10 μg/ml) for 8 h, and the total RNA was isolated for traditional RT-PCR or real time PCR. The cells were also treated for 8 h with LPS (100 ng/ml), TNF-α (10 ng/ml), or LPS (100 ng/ml) plus IFN-γ (50 units/ml) for comparison purposes. The mRNA levels of chemokines (CCL4, CCL20, CXCL2, and CXCL10) and other inflammatory genes (IL-6, COX-2, iNOS, and PIAS3) were determined by traditional RT-PCR (*A–D*) or real time PCR (*E*). β-Actin or GAPDH was used as an internal control. The results are one representative of more than three independent experiments (*A–D*) or means ± S.D. ($n = 3$) (*E*).

1-2 mouse ascites fluid (Sigma)) and HRP-conjugated secondary antibodies (anti-goat, anti-rabbit, and anti-mouse IgG; Amersham Biosciences), followed by ECL detection (Amersham Biosciences).

Nuclear Extraction and EMSA—Nuclear extracts were prepared from astrocyte cultures, and the electrophoretic mobility shift assay was conducted as described previously (45). Nuclear extracts (5 μg) were mixed with double-stranded NF-κB oligonucleotide (5′-GAT CCC AAC GGC AGG GGA-3′; Promega), which was end-labeled with [γ-^{32}P]dATP using T4 polynucleotide kinase. Labeled nucleic acids were purified using a mini Quick Spin column (Roche Applied Science). The binding reactions were performed at 37 °C for 30 min in 30 μl of reaction buffer containing 10 mM Tris-HCl, pH 7.5, 100 mM NaCl, 1 mM EDTA, 4% glycerol, 1 μg of poly(dI-dC), and 1 mM DTT. For the supershift assay, antibody against p65 subunit of NF-κB (Santa Cruz Biotechnology Inc., Santa Cruz, CA) was coincubated with nuclear extracts in the reaction mixture for 30 min at 4 °C before adding the radiolabeled probe. The specificity of binding was examined by competition with the 80-fold unlabeled oligonucleotide. DNA-protein complexes were separated from the unbound DNA probe on native 5% polyacrylamide gels at 180 V in 0.5× Tris-boric acid-EDTA buffer. The gels were vacuum-dried for 1 h at 80 °C and exposed to x-ray film at −70 °C for 24 h.

Assessment of Cytotoxicity by 3-[4,5-Dimethylthiazol-2-yl]-2,5-diphenyltetrazolium Bromide Assay—Cells (5×10^4 cells in 200 μl/well) were seeded in 96-well plates and treated with various stimuli for the specific time periods. After treatment, the medium was removed and 3-[4,5-dimethylthiazol-2-yl]-2,5-diphenyltetrazolium bromide (0.5 mg/ml) was added, followed by incubation at 37 °C for 2 h in a CO_2 incubator. After insoluble crystals were completely dissolved in Me_2SO, absorbance at 570 nm was measured by using a microplate reader (Anthos Labtec Instruments, Wals, Austria).

Nitrite Quantification—Astrocyte cultures were treated with stimuli in 96-well plates, and then NO_2^- in culture media was measured to assess NO production levels by the Griess reaction as described previously (18). Fifty microliters of sample aliquots were mixed with 50 μl of Griess reagent (1% sulfanilamide, 0.1% naphthylethylene diamine dihydrochloride, 2% phosphoric acid) in 96-well plates and incubated at 25 °C for 10 min. The

absorbance at 540 nm was measured with a microplate reader (Anthos Labtec Instruments). $NaNO_2$ was used as the standard to calculate NO_2 concentrations.

Mouse Breeding and Maintenance—LCN2-deficient mice were a gift from Dr. Shizuo Akira (Osaka University, Japan). LCN2 wild-type ($LCN2^{+/+}$) and LCN2-deficient ($LCN2^{-/-}$) mice were back-crossed for eight to ten generations onto to the C57BL/6 background to generate homozygote and heterozygote animals as described previously (9, 46). Genotype was confirmed by PCR analysis of genomic DNA (46). The C57BL/6 mice that were used for breeding were purchased from the Samtako Co. $LCN2^{-/-}$ mice were age- and sex-matched with C57BL/6 controls.

Cortical Stab Wound Injury Model—Cortical stab wound injury was performed as described previously (47). The mice were anesthetized with enflurane and placed in a stereotaxic instrument. A midline incision was made through the scalp, and the skin was retracted laterally. The hole was drilled over the right cerebral hemisphere, exposing the dura. A 30-gauge needle was inserted into the cortical site coordinated as 0.5 mm anterior to bregma, −3 mm lateral to bregma, and 1 mm below the skull and left in place for 5 min. After the needle was removed, the mice were allowed to recover and returned to their cages at 2 days post-injury (dpi). For immunohistochemical analysis, the animals were anesthetized by ether and transcardially perfused with 4% paraformaldehyde in PBS at 2 dpi. The brains were postfixed and cryo-protected by 30% sucrose in PBS. The fixed brains were embedded in optimal cutting temperature compound (Tissue-Tek; Sakura Finetechnical Co., Tokyo, Japan) for frozen section and then cut into 12-μm-thick coronal sections. After PBS washing, the sections were permeabilized in 0.1% Triton X-100 and blocked with 1% BSA and 5% normal donkey serum. The sections were incubated with mouse monoclonal anti-GFAP antibody (1:500 dilution; Biogenex) at 4 °C overnight. The sections were then incubated with secondary antibodies (donkey FITC-conjugated anti-rabbit IgG antibody (1:200 dilution; Jackson Immunoresearch Laboratories, West Grove, PA)). Data acquisition and immunohistological intensity measurement of GFAP staining was performed with a National Institutes of Health ImageJ program. Composite images of stained section were Fast Fourier transform band-pass filtered to eliminate low frequency drifts (>20 pixels = 50 mm) and high frequency noises (<1 pixel = 2.5 mm). The image was binary thresholded at 50% of the background level, and then the particles were converted to a subthreshold image area with the size less than 300 and larger than 20 pixels, which was judged as GFAP-positive cells. The range (20–300 pixels) was obtained from the analyzed size of GFAP-positive cells from six sections for each experimental group. To count the GFAP-positive cells, five squares (200 μm × 200 μm) were placed to peri-region of injection in the subthreshold image of the six independent sections. The cells in the five squares were counted and statistically analyzed.

Mouse Models of Neuroinflammation—Either intracortical or intracerebroventricular injection of LPS was done to induce brain inflammation in mice. $LCN2^{+/+}$ or $LCN2^{-/-}$ mice received an intracortical injection of 1 μl (5 μg) of LPS. Briefly, animals (body weight of about 30 g) were placed in a stereotaxic

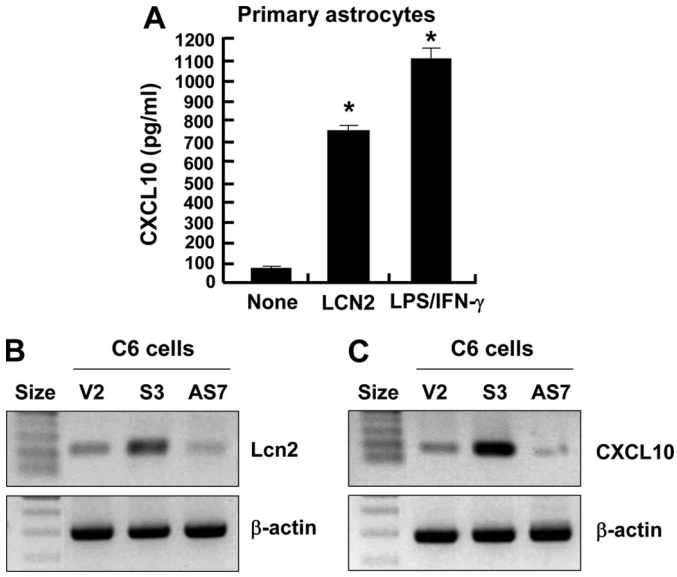

FIGURE 2. **An increase of CXCL10 expression by LCN2 in astrocytes.** Astrocytes were incubated with the recombinant LCN2 protein (10 μg/ml) or LPS (100 ng/ml) plus IFN-γ (50 units/ml) for 24 h. The amounts of CXCL10 protein in the culture media were measured by specific ELISA (*A*). The results are means ± S.D. ($n = 3$). *, $p < 0.05$ compared with the untreated control. The stable overexpression or knockdown of *lcn2* expression was achieved by transfection with sense or antisense *lcn2* cDNA in C6 rat glioma cells. The increased or decreased *lcn2* expression in the stable transfectants (*S3*, *lcn2* sense transfectant; *AS7*, *lcn2* antisense transfectant) compared with cells transfected with an empty vector (*V2*) was confirmed by RT-PCR (*B*). Changes in the CXCL10 mRNA levels in the stable transfectants were also assessed by RT-PCR (*C*). β-Actin was used as an internal control. The results are one representative of more than three independent experiments.

instrument (Stoelting, Wood Dale, IL) and given an intracortical injection of LPS using a 5-μl Hamilton microsyringe fitted with a 26-gauge needle that was inserted into the cortical site (coordination 0.5 mm anterior to bregma, −3 mm lateral to bregma, and 1 mm below the skull) under brief enflurane anesthesia. Intracerebroventricular injection was delivered as previously described (48). After brief enflurane anesthesia, the mice were placed in a stereotaxic instrument and given an injection at the site coordinated as 0.2 mm anterior to bregma, −1 mm lateral, and 2.5 mm depth from the skull using a 5-μl Hamilton microsyringe fitted with a 26-gauge needle. The injection volume was 3 μl (15 μg) of LPS. Flow rate of injection was 0.1 μl/min. At 2 dpi, for immunohistochemical analysis, the animals were anesthetized and transcardially perfused with 4% paraformaldehyde. The brains were postfixed and cryo-protected. The fixed brains were embedded in optimal cutting temperature compound (Tissue-Tek; Sakura Finetechnical Co., Tokyo, Japan) for frozen section and then cut into 12-μm-thick coronal sections. After PBS washing, the sections were permeabilized in 0.1% Triton X-100 and blocked with 1% BSA and 5% normal donkey serum. The sections were incubated with rabbit polyclonal anti-LCN2 antibody (1:50 dilution; Santa Cruz), or mouse monoclonal anti-GFAP antibody (1:500 dilution; Biogenex) at 4 °C overnight. The sections were then incubated with secondary antibodies (donkey FITC-conjugated anti-rabbit IgG antibody (1:200 dilution; Jackson Immunoresearch Laboratories, West Grove, PA) or donkey Cy™3-conjugated anti-mouse IgG antibody (1:200 dilution;

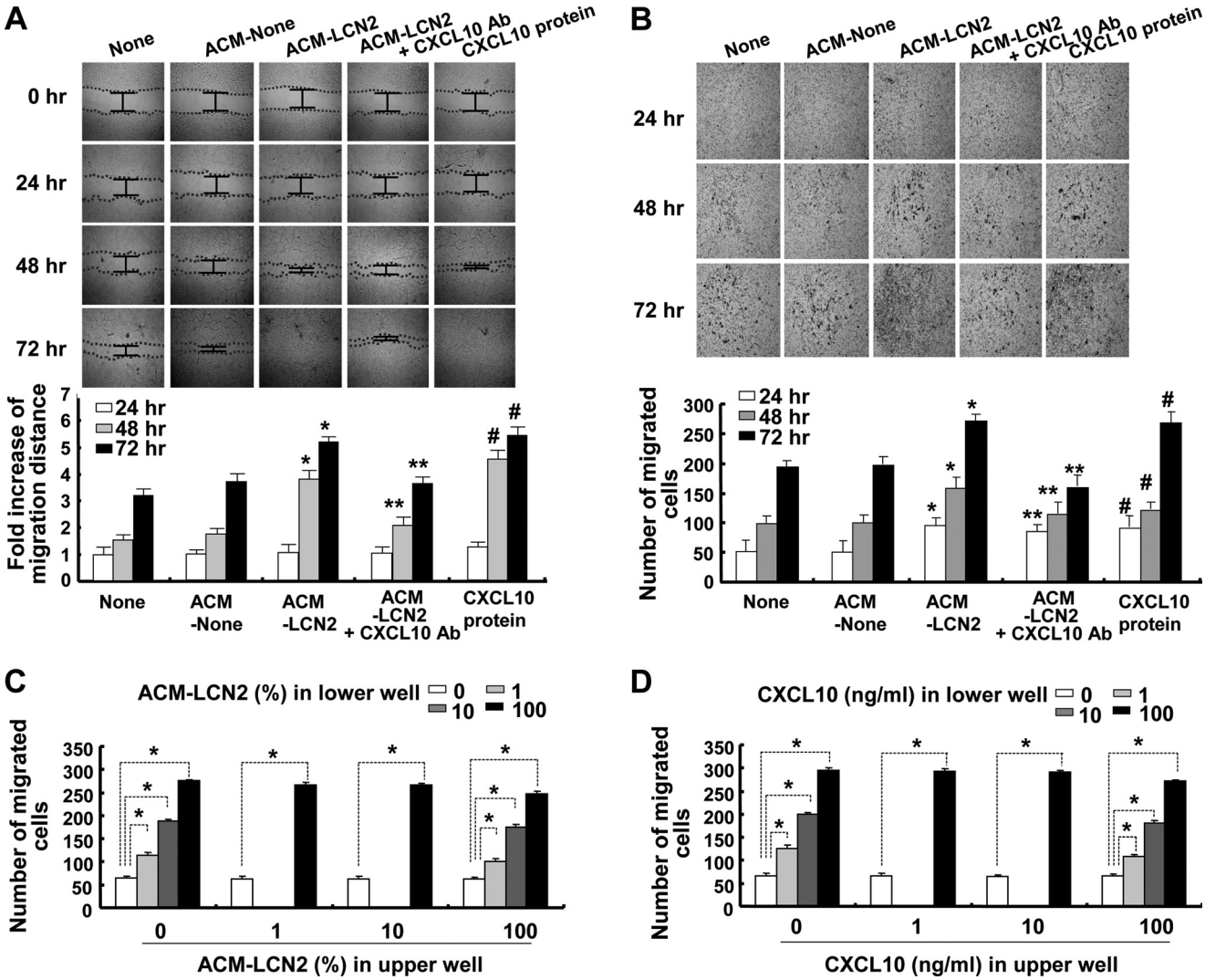

FIGURE 3. **Astrocyte-derived CXCL10 promoted the migration of astrocytes.** Astrocytes (1×10^4 cells/upper well) were exposed to LCN2 (10 μg/ml)-stimulated ACM or the recombinant CXCL10 protein (10 ng/ml) in the presence or absence of CXCL10 neutralizing antibody (CXCL10 Ab; 10 ng/ml) as indicated. *ACM-None*, untreated ACM; *ACM-LCN2*, LCN2-treated ACM (see "Experimental Procedures" for the preparation of ACM). After treatment for the indicated time periods, either wound healing assay (*A*) or the Boyden chamber assay (*B*) was performed to evaluate cell migration. A representative microscopic image for each condition was shown (magnification, ×100) (*upper*). The quantification of cell migration was done by either measuring the degree of wound closure (wound healing assay) or enumerating the migrated cells (Boyden chamber assay) as described under "Experimental Procedures" (*lower*). The results are means ± S.D. ($n = 3$). *, $p < 0.05$ compared with *ACM-None* at the same time point; **, $p < 0.05$ compared with *ACM-LCN2* at the same time point; #, $p < 0.05$ compared with the untreated control (*None*) at the same time point. For the checkerboard analysis, migration of astrocytes (2×10^4 cells/upper well) in response to the indicated concentrations of ACM-LCN2 (*C*) and the recombinant CXCL10 protein (*D*) placed in upper and/or lower well was determined using the Boyden chamber assay. The quantification of cell migration was done by enumerating the migrated cells after 48 h as described under "Experimental Procedures." The results are the means ± S.D. ($n = 3$). *, $p < 0.05$ between the treatments indicated.

TABLE 3

Checkerboard analysis for promigratory effects of ACM-LCN2 in astrocytes

ACM-LCN2 was added to the upper and/or lower wells of the Boyden chambers for the checkerboard analysis. After cells were incubated at 37 °C under 5% CO_2 for 48 h, cell migration was assessed as described under "Experimental Procedures." NT, not tested.

	ACM-LCN2 (%) in upper well			
ACM-LCN2 (%) in lower well	0	1	10	100
0	64.2 ± 4.2	62.2 ± 5.4	63.1 ± 5.3	62.4 ± 3.8
1	114.4 ± 5.1	NT	NT	101.2 ± 4.6
10	189.1 ± 3.6	NT	NT	175.7 ± 4.5
100	275.3 ± 2.6	266.2 ± 6.1	265.8 ± 4.4	248.1 ± 5.1

Jackson Immunoresearch Laboratories)). The counter stain was performed using Vectashield mounting medium with DAPI (Vector Laboratories, Burlingame, CA). To count the GFAP-positive cells, five 100-μm × 100-μm squares in each brain section were randomly chosen (Olympus BX51) (original magnification, ×400–1000). The same position in the five independent brain sections was visualized. The cells in the five squares were counted and statistically analyzed. The number of GFAP-positive cells/mm^2 was calculated according to the size of the specific brain area. The results were

TABLE 4

Checkerboard analysis for promigratory effects of recombinant CXCL10 protein in astrocytes

The recombinant CXCL10 protein was added to the upper and/or lower wells of the Boyden chambers for the checkerboard analysis. After cells were incubated at 37 °C under 5% CO_2 for 48 h, cell migration was assessed as described under "Experimental Procedures." NT, not tested.

CXCL10 (ng/ml) in lower well	CXCL10 (ng/ml) in upper well			
	0	1	10	100
0	67.3 ± 4.6	66.7 ± 5.2	65.2 ± 3.4	66.1 ± 3.6
1	126.4 ± 6.2	NT	NT	108.8 ± 3.1
10	198.9 ± 4.8	NT	NT	181.1 ± 4.8
100	294.3 ± 6.3	293.6 ± 5.2	291.1 ± 4.6	271.3 ± 3.5

presented as the means ± S.D. ($n = 3$). Quantification of GFAP-positive cells was done using the ImageJ program (National Institutes of Health Image).

Statistical Analysis—All of the data were presented as the means ± S.D. from three or more independent experiments, unless stated otherwise. Statistical comparisons between different treatments were done by either a Student's *t* test or one-way analysis of variance with Dunnett's multiple-comparison tests by using the *SPSS* version 18.0K program (SPSS Inc., Chicago, IL). Differences with a value of $p < 0.05$ were considered to be statistically significant.

RESULTS

LCN2 Up-regulates Chemokine Expression in the CNS—We have previously demonstrated that LCN2 plays a central role in reactive astrocytosis (18). To gain a deeper understanding of how LCN2 participates in the phenotypic transformation of astrocytes, we have analyzed the global gene expression profile of LCN2-stimulated astrocytes by DNA microarray analysis (Table 2). A complete list of genes with differential expression is available in the Gene Expression Omnibus under accession number GSM392157. Chemokines constituted the major group of genes up-regulated by LCN2. Among 40 genes that showed more than a 2-fold increase, 10 genes (25%) belonged to the chemokine family. Traditional RT-PCR or real time PCR analysis was conducted for individual chemokine genes to validate the microarray results (Fig. 1). The up-regulation of CXCL2/GRO-β and CXCL10/IP-10 was confirmed by RT-PCR in astrocytes treated with LCN2 (Fig. 1*A*). The induction of other inflammatory genes, such as IL-6, COX-2, and iNOS, was also confirmed (Fig. 1*A*). The cells were also treated with LPS, LPS/IFN-γ, or TNF-α for comparison purposes. Different stimulatory conditions were used for the different CNS cell types because of their specific stimulatory requirements. LCN2 induced the down-regulation of 475 genes with greater than a 2-fold change, among which a decrease in the protein inhibitor of activated STAT3 (PIAS3) expression was confirmed (Fig. 1*A*). Up-regulated or down-regulated genes with greater than 1.5- or 3.5-fold changes, respectively, are listed in Table 2. In the next set of experiments, we explored the possibility that LCN2 may up-regulate the chemokine gene expression in other cell types that are present in the CNS. Most chemokines analyzed also showed the increased expression in LCN2-treated microglia, endothelial cells, and neuronal cells (Fig. 1, *B–D*). Expression of some of the chemokines/cytokines was also analyzed by real time PCR, which gave a similar result (Fig. 1*E*). The results suggest that LCN2 may act as a general chemokine inducer in the CNS. LCN2 concentration used in the current study is

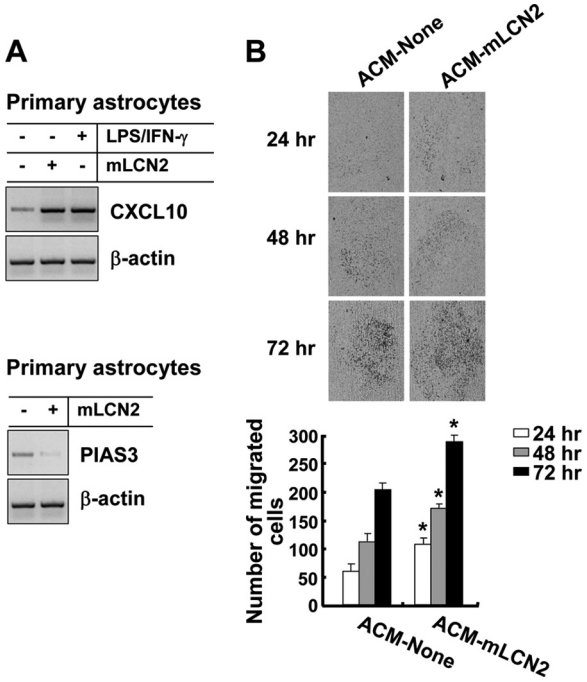

FIGURE 4. **The effects of LCN2 protein expressed in mammalian cells (mLCN2) on the chemokine gene expression and cell migration in astrocytes.** Astrocytes were treated with the NSO murine melanoma cell-derived mouse LCN2 protein (10 μg/ml; mLCN2) for 8 h, and the total RNA was isolated for traditional RT-PCR. The cells were also treated for 8 h with LPS (100 ng/ml) plus IFN-γ (50 units/ml) for comparison purposes. The mRNA levels of CXCL10 and PIAS3 were determined by traditional RT-PCR (*A*). β-Actin was used as an internal control. The results are one representative of more than three independent experiments. Astrocytes (1×10^4 cells/upper well) were exposed to the melanoma cell-expressed LCN2 protein (10 μg/ml; mLCN2)-stimulated astrocyte-conditioned media (ACM-mLCN2). Astrocytes placed in the Boyden chambers were then incubated at 37 °C for 24–72 h to evaluate cell migration (*B*). A representative microscopic image for each condition was shown (magnification, ×100) (*upper*). *ACM-None*, untreated ACM; *ACM-mLCN2*, mLCN2-treated ACM. The quantification of cell migration was done by enumerating the migrated cells as described under "Experimental Procedures" (*lower*). The results are the means ± S.D. ($n = 3$). *, $p < 0.05$ compared with *ACM-None* at the same time point.

based on the previous reports. We and others have shown that LCN2 protein concentrations in the blood of normal mice are ~100 ng/ml (or 4 nM) (9, 10). LCN2 is one of the most highly induced molecules in inflammatory disorders, whose concentrations reach 30 μg/ml in the blood and 40 μg/ml in the urine (10, 49). Locally, even higher levels may be achieved in pathologic conditions. The recombinant GST protein, which was purified in the process of LCN2 preparation (18), was used as a control. The GST protein did not up-regulate chemokine expression (data not shown). The constitutive or inducible expression of *lcn2* and its receptors has been either previously demonstrated for microglia (17) and astrocytes (18) or shown in

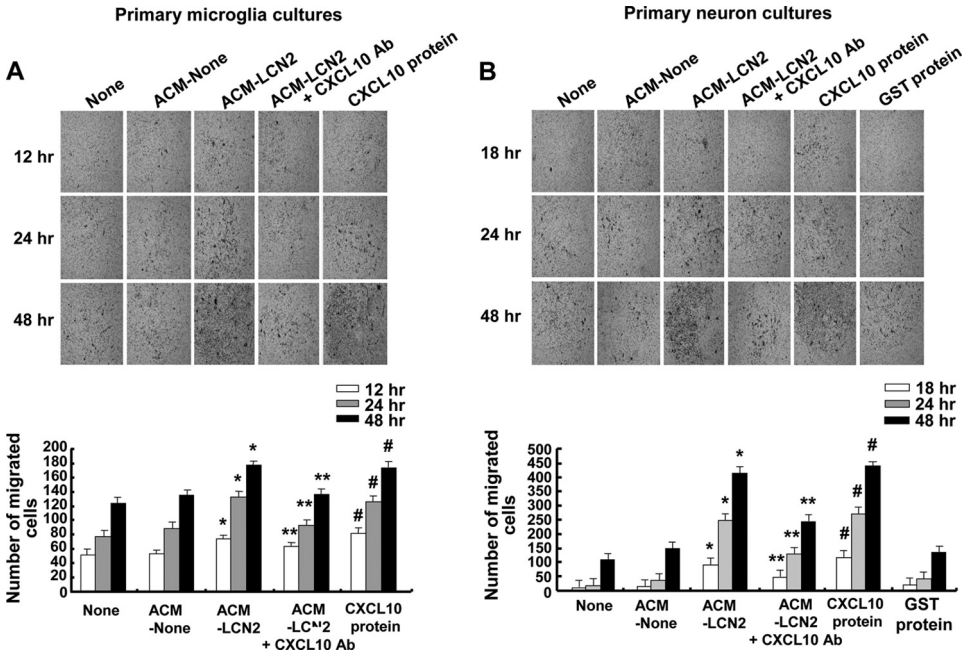

FIGURE 5. **Astrocyte-derived CXCL10 promoted the migration of microglia and neuron cells.** Microglia (1×10^4 cells/upper well) (*A*) or neuron cells (1×10^4 cells/upper well) (*B*) were exposed to LCN2 (10 μg/ml)-stimulated ACM or the recombinant CXCL10 protein (10 ng/ml) in the presence or absence of CXCL10 neutralizing antibody (10 ng/ml) as indicated. Microglia or neuron cells placed in the Boyden chambers were incubated at 37 °C for 12–48 or 18–48 h, respectively, to evaluate cell migration. The GST protein (10 μg/ml) was used as a control for the recombinant LCN2 protein. A representative microscopic image for each condition is shown (magnification, ×100) (*upper*). *ACM-None*, untreated ACM; *ACM-LCN2*, LCN2-treated ACM. The quantification of cell migration was done by enumerating the migrated cells as described under "Experimental Procedures" (*lower*). The results are the means ± S.D. ($n = 3$). *, $p < 0.05$ compared with *ACM-None* at the same time point; **, $p < 0.05$ compared with *ACM-LCN2* at the same time point; #, $p < 0.05$ compared with the untreated control (*None*) at the same time point.

this study for endothelial cells and neuronal cells (supplemental Fig. S1, *A–D*). The results suggest that LCN2 may directly act on these cell types to up-regulate chemokine expression. Recently, two cellular receptors for LCN2 have been identified. Megalin, a member of the low density lipoprotein receptor family, has been shown to bind human LCN2 with high affinity and to mediate its endocytosis (50). Brain type organic cation transporter (24p3R) is another cell surface receptor for mouse *lcn2*, which has been shown to mediate apoptosis or iron uptake (1). LCN2 may act on these receptors to initiate its activity.

Chemokines Mediate LCN2-induced Cell Migration—Based on the RT-PCR analysis of chemokines, CXCL10 showed the most significant change in the mRNA expression levels in LCN2-stimulated astrocytes. LCN2 enhancement of CXCL10 expression at protein levels was confirmed by ELISA (Fig. 2*A*). It has been previously shown that CXCL10 protein concentrations in the astrocytes are 300–1000 pg/ml (51), which is consistent with the current results. LCN2 induction of CXCL10 expression in astrocytes was further confirmed by the overexpression or knockdown of *lcn2* expression in the C6 glioma cell line (Fig. 2, *B* and *C*). C6 glial cells with an increased or decreased expression of *lcn2* were generated by stable transfection with sense or antisense *lcn2* cDNA (18). Levels of *lcn2* expression were correlated with those of CXCL10, supporting that endogenous LCN2 up-regulates CXCL10 expression in astrocytes. Moreover, the LCN2-up-regulated CXCL10 expression was consistently found in microglia, endothelial cells, and neuronal cells, as well as in astrocytes (Fig. 1). Of several chemokines, CXCL10 expression was most strongly up-regulated by LCN2 in all of these cell types (Fig. 1). These results prompted us to hypothesize that chemokines, such as CXCL10, may mediate LCN2-induced cell migration. LCN2 is an autocrine mediator of reactive astrocytosis (18). Thus, LCN2-up-regulated chemokines may also be responsible for the morphological features of reactive astrocytosis phenotype. This hypothesis was tested by evaluating the effect of LCN2-treated ACM on the CNS cell migration and morphology. The cell migration assay, such as *in vitro* wound healing assay (Fig. 3*A*) and the Boyden chamber assay (Fig. 3*B*), revealed that LCN2-treated ACM (ACM-LCN2) augmented astrocyte migration, which was inhibited or mimicked by CXCL10 neutralizing antibody or the recombinant CXCL10 protein, respectively (Fig. 3, *A* and *B*). In the wound healing assay, astrocytes treated with ACM-LCN2 or the recombinant CXCL10 protein became confluent at 72 h. Checkerboard analysis (Fig. 3, *C* and *D*, and Tables 3 and 4) was performed with different dilutions of ACM-LCN2 and the recombinant CXCL10 protein to determine whether the ACM-LCN2 and the recombinant CXCL10 protein cause chemotaxis (directed movement) or chemokinesis (random movement) of the astrocytes. Maximal migration occurred when high concentrations of the ACM-LCN2 and the recombinant CXCL10 protein were placed in the lower chamber, and no significant increase in migration was observed when equal concentrations of the ACM-LCN2 and the recombinant CXCL10 protein were placed on both sides of the chamber, thereby indicating that the ACM-LCN2 and the recombinant CXCL10 protein were strongly chemotactic to the astrocytes (Fig. 3, *C* and *D*, and Tables 3 and 4). The GST protein used as a control was without effect (data not shown). The LCN2 regulation of CXCL10 or PIAS3 expression in astrocytes was con-

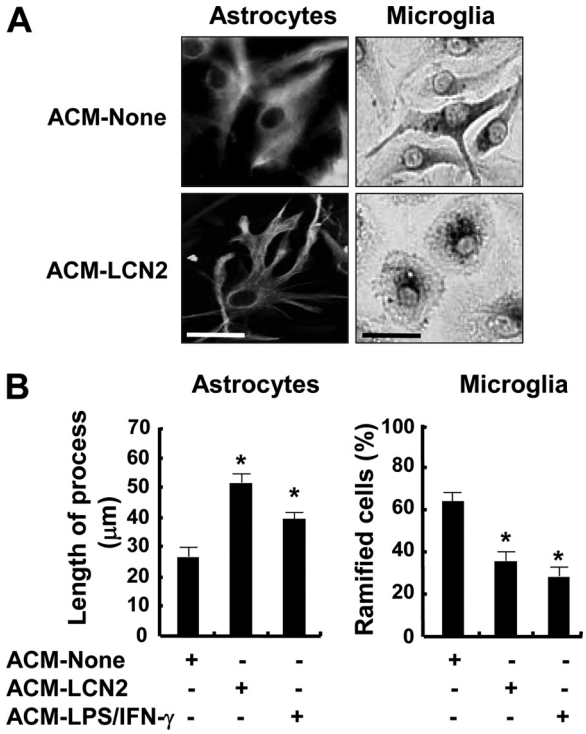

FIGURE 6. **The effect of LCN2-treated ACM on the morphology of astrocytes and microglia.** ACM was prepared after the treatment of primary astrocytes with LCN2 (10 μg/ml) for 24 h. The addition of LCN2-treated ACM (*ACM-LCN2*) induced morphological changes in primary astrocytes and primary microglia cultures after 24 h (*A*). Primary astrocytes were stained with GFAP antibody (original magnification, ×400), followed by the incubation with anti-mouse IgG-FITC-conjugated secondary antibody. Primary microglia were stained with the peroxidase-labeled isolectin B4 (original magnification, ×100), followed by incubation with diaminobenzidine tetrahydrochloride. *Scale bars*, 25 μm. The length of the longest process in each astrocyte or the percentage of ramified microglia was assessed by examining several randomly chosen microscopic fields (*B*). The results are the means ± S.D. ($n = 3$). *, $p < 0.05$; compared with the untreated ACM control (*ACM-None*).

firmed by using murine LCN2 protein expressed in mammalian cells (mLCN2) (Fig. 4*A*). The mLCN2-treated ACM (ACM-mLCN2) also promoted the migration of astrocytes (Fig. 4*B*), indicating that LCN2 proteins expressed in bacteria and mammalian cells have the same effects on the chemokine expression and cell migration. The results indicate that CXCL10, among the chemokines up-regulated by LCN2, may account for most, if not all, cell migration-promoting activity of LCN2. Similar results were obtained for microglia or neuronal cultures (Fig. 5, *A* and *B*), indicating that LCN2-up-regulated chemokines promote the migration of both glia and neurons. The expression of the CXCL10 receptor, CXCR3, was detected in primary astrocytes, primary microglia, or primary cortical neuron cultures (supplemental Fig. S1*E*), supporting an important role for CXCL10/CXCR3 in CNS cell migration. ACM-None, ACM-LCN2, CXCL10 protein, or mLCN2 protein did not significantly affect cell proliferation or viability of primary astrocytes, microglia, or neuron cultures as determined by 3-[4,5-dimethylthiazol-2-yl]-2,5-diphenyltetrazolium bromide assays (data not shown), indicating that the data in Figs. 3–5 are independent of the effects on cell proliferation or cell death. Effects of ACM prepared after the LCN2 treatment on cell morphology were next determined. ACM-LCN2 also induced morphological changes in glia (Fig. 6) and neurons (data not shown): the cellular process extension was observed for astrocytes and neurons, whereas amoeboid transformation of microglia was induced. As far as astrocytes are concerned, the morphological change reflects phenotypic alteration during reactive astrocytosis. This further supports that LCN2 induces reactive astrocytosis and CNS cell migration via the secretion of chemokines, such as CXCL10.

STAT3 and NF-κB Mediate LCN2-up-regulated CXCL10 Expression in Astrocytes—We next examined signaling pathways that led to CXCL10 up-regulation in LCN2-exposed astrocytes. Based on the results of the microarray analysis that showed the down-regulation of PIAS3 by LCN2, we tested the involvement of the STAT3 signaling in the LCN2-up-regulated CXCL10 expression. LCN2 alone induced phosphorylation of STAT3 at serine 727 and tyrosine 705 (Fig. 7*A*). The LCN2-induced STAT3 phosphorylation at the two amino acid residues showed slightly different time kinetics (Fig. 7*B*). LCN2 also enhanced STAT3 phosphorylation induced by phorbol 12-myristate 13-acetate, ATP, and IFN-γ. The total levels of STAT3 proteins were not affected under this condition. AG490 (JAK2/STAT3-specific inhibitor), but not piceatannol (JAK1/STAT1-specific inhibitor), significantly attenuated LCN2-induced CXCL10 protein production as determined by ELISA (Fig. 7*C*). In contrast, LPS/IFN-γ-induced CXCL10 production was suppressed by both AG490 and piceatannol, indicating the importance of both JAK2/STAT3 and JAK1/STAT1 pathways under this condition, which was used for comparison purposes. The level of LCN2-induced CXCL10 production was comparable with that of LPS-induced CXCL10 and was not abolished by polymyxin B treatment, ruling out the possibility of LPS contamination in the process of recombinant LCN2 preparation (supplemental Fig. S2, *B* and *C*). mLCN2 of mammalian origin was also used to further exclude the possibility of LPS contamination (Fig. 4). Polymyxin B, AG490, and piceatannol did not affect cell viability at the concentrations used in the current study (supplemental Fig. S2, *A*, *D*, and *E*). Taken together, these results indicate that LCN2 up-regulates CXCL10 production partly through the JAK2/STAT3 signaling pathway in astrocytes. The LCN2 activation of the JAK2/STAT3 pathway may be facilitated by either the down-regulation of inhibitory PIAS3 expression or the up-regulation of IL-6 expression; this is based on the microarray analysis showing that LCN2 down-regulates PIAS3 and up-regulates IL-6 expression (Fig. 1*A*). Previously, PIAS3 proteins had blocked the DNA binding activity of STAT3 and inhibited STAT3-mediated gene activation (52), whereas IL-6 is known to stimulate the STAT3 pathway that is also a critical component of reactive astrocytosis (53). In the mean time, LCN2-induced GFAP expression was also diminished by AG490 (Fig. 7*D*), indicating that JAK2/STAT3 signaling may also be involved in LCN2-induced GFAP expression and the process extension of astrocytes during reactive astrocytosis. Because NF-κB is a canonical pathway that is involved in numerous inflammatory gene expression, the effect of LCN2 on NF-κB signaling was also determined. LCN2 strongly induced NF-κB activation (Fig. 7*E*). Additionally, LCN2-induced NO production was reduced by pyrrolidine dithiocarbamate (NF-κB inhibitor), further supporting that LCN2 induces astrocyte NO production and activation through

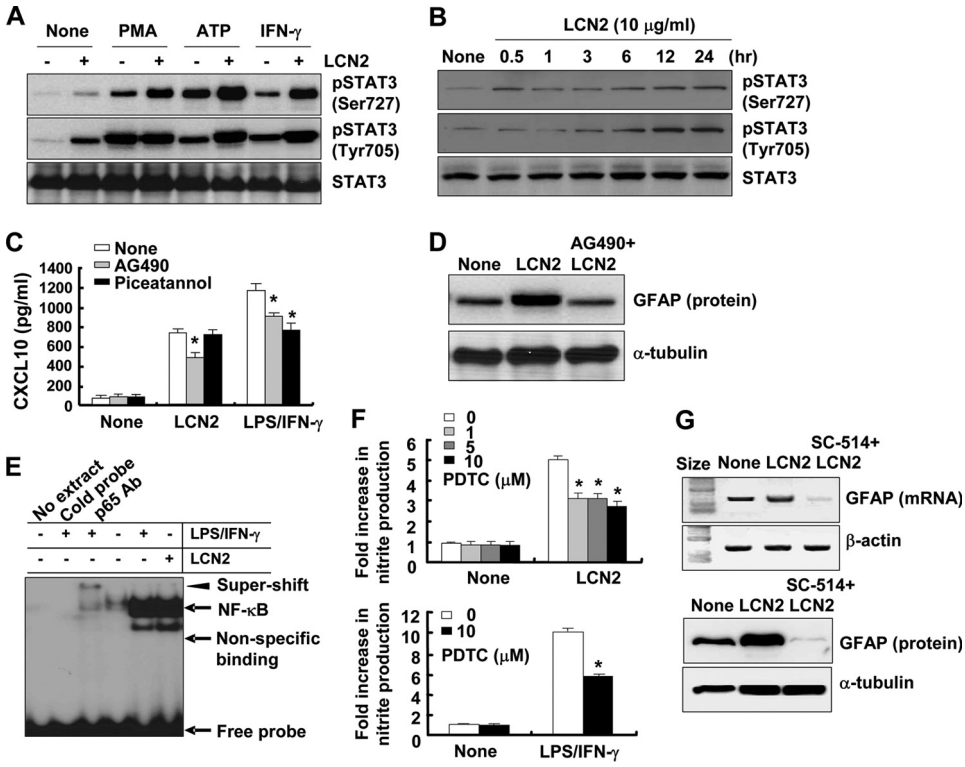

FIGURE 7. **JAK2/STAT3 and IKK/NF-κB mediated LCN2 up-regulation of CXCL10 and GFAP expression in astrocytes.** Astrocytes were pretreated with the recombinant LCN2 protein (10 μg/ml) for 24 h prior to the treatment with phorbol 12-myristate 13-acetate (100 μg/ml), ATP (3 mM), or IFN-γ (50 units/ml) for 30 min. Astrocytes were also exposed to phorbol 12-myristate 13-acetate (*PMA*), ATP, or IFN-γ for 30 min without LCN2 pretreatment (*A*). Alternatively, astrocytes were treated with LCN2 for 0.5–24 h for the time kinetics analysis (*B*). The levels of phosphorylated STAT3 (pSTAT3 at Ser^{727} or Tyr^{705}) or total STAT3 protein were then evaluated by Western blot analysis. The results are one representative of more than three independent experiments. Alternatively, astrocytes were pretreated with AG490 (JAK2/STAT3-specific inhibitor, 50 μM) or piceatannol (JAK1/STAT1-specific inhibitor, 50 μM) for 30 min prior to the treatment with the recombinant LCN2 protein (10 μg/ml) or LPS (100 ng/ml) plus IFN-γ (50 units/ml) for 24 h. The secreted CXCL10 protein was measured by specific ELISA (*C*). The results are the means ± S.D. ($n = 3$). *, $p < 0.001$ compared with the treatment without inhibitors. Astrocytes were pretreated with AG490 for 30 min prior to the treatment with the recombinant LCN2 protein (10 μg/ml) for 24 h. The expression of GFAP protein levels was assessed by Western blot analysis, respectively (*D*). After astrocytes were treated with the recombinant LCN2 protein (10 μg/ml) or LPS (100 ng/ml) plus IFN-γ (50 units/ml) for 1 h, an EMSA analysis of the nuclear extracts was conducted by using a ^{32}P-labeled NF-κB oligonucleotide probe (*E*). Binding specificity was determined by the supershift assay using antibody against p65 (*p65 Ab*) or its coincubation with an unlabeled probe containing the NF-κB binding sequence (*cold probe*) to compete with the labeled oligonucleotide. The results are one representative of more than three independent experiments. Primary astrocytes were pretreated with pyrrolidine dithiocarbamate (*PTDC*, NF-κB-specific inhibitor; 0–10 μM) for 30 min prior to their treatment with the recombinant LCN2 protein (10 μg/ml) or LPS (100 ng/ml) plus IFN-γ (50 units/ml) for 24 h (*F*). The concentration of nitrite in the culture media was measured by the Griess reagent. The results are the means ± S.D. ($n = 3$). *, $p < 0.001$ compared with the LCN2 or LPS/IFN-γ treatment alone. The astrocytes were pretreated with SC-514 (IKK-specific inhibitor, 10 μM) for 30 min prior to the treatment with the recombinant LCN2 protein (10 μg/ml) for 8–24 h. The expression of GFAP at mRNA or protein levels after 8 or 24 h was then assessed by RT-PCR or Western blot analysis, respectively (*G*).

NF-κB (Fig. 7*F*). NO may be involved in the amplification of LCN2-induced GFAP expression, because NO had previously enhanced GFAP expression in astrocytes (18, 54). Studies using pharmacological inhibitors, such as pyrrolidine dithiocarbamate and SC-514 (IKK-specific inhibitor), indicated that the LCN2-induced up-regulation of CXCL10 production and GFAP expression involved the IKK/NF-κB pathway (Fig. 7*G*). SC-514 treatment reduced GFAP mRNA and protein levels below the basal expression, suggesting that the constitutive expression of GFAP may also require NF-κB pathway. SC-514 also decreased LCN2-mediated CXCL10 protein production in primary astrocytes, as determined by ELISA: LCN2-up-regulated CXCL10 production was inhibited 37.50 ± 0.84% by SC-514 (10 μM), whereas LPS/IFN-γ-up-regulated CXCL10 production was inhibited 26.31 ± 0.72% by SC-514. The partial inhibition suggests that other pathways may also participate in the LCN2 effects on CXCL10 production. SC-514 did not affect cell viability at the concentration used in this study (supplemental Fig. S2*F*). Collectively, JAK2/STAT3 and NF-κB seem to be major components of signal transduction pathways that lead to the LCN2 up-regulation of CXCL10 and GFAP expression in astrocytes.

Functional Analysis of LCN2 in Vivo Using Mouse Brain Injury and Neuroinflammation Models—To investigate the role of LCN2 in CNS cell migration *in vivo*, we used mouse models of brain injury and inflammation. We first investigated the expression of LCN2 in adult mouse tissues from LCN2 wild-type ($LCN2^{+/+}$), LCN2 heterozygous ($LCN2^{+/-}$), and LCN2-deficient ($LCN2^{-/-}$) mice. As described previously (12, 55, 56), the LCN2 expression was detected in brain, lung, liver, and kidney of $LCN2^{+/+}$ mice, but not $LCN2^{-/-}$ mice; the expression level was dependent on the gene dosage (supplemental Fig. S3). We next investigated the role of LCN2 in the well established models of brain injury and inflammation (cortical stab wound injury model as well as intracortical and intracerebroventricular (icv) injection of LPS). Adult mice ($LCN2^{+/+}$ and $LCN2^{-/-}$) received cortical stab wound injuries. The animals were then perfused, and brain tissue was prepared for

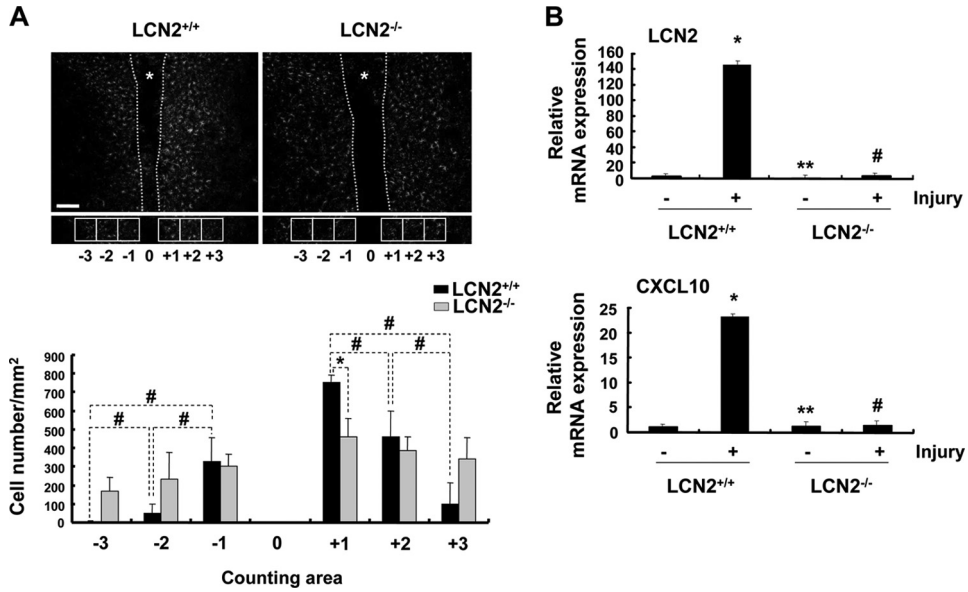

FIGURE 8. **Role of LCN2 in astrocyte migration and CXCL10 induction in cortical stab wound injury model.** Cortical stab wound injury was performed with LCN2 wild-type ($LCN2^{+/+}$) or LCN2-deficient mice ($LCN2^{-/-}$) (*A*, *upper*). At 2 dpi, the mice were sacrificed, and cryosections were immunostained with antibodies against GFAP. The *asterisk* indicates stab wound injury site. The *boxes* indicate 200-μm × 200-μm squares placed for cell counting. Immunohistochemistry results showed that GFAP-positive cells in the peri-injury region were observed in both $LCN2^{+/+}$ and $LCN2^{-/-}$ mice. A significant decrease in the number of GFAP-positive cells was observed in the immediate vicinity of injury site in $LCN2^{-/-}$ mice (*A*, *lower panel*). The results are one representative of more than three independent experiments. *Scale bars*, 200 μm. The values are the means ± S.D. from three different animals and six independent sections/animal. *, $p < 0.05$ compared with $LCN2^{-/-}$ mice in the same counting area; #, $p < 0.05$ between the values indicated. The mRNA levels of *lcn2* (*upper panel*) and CXCL10 (*lower panel*) in $LCN2^{+/+}$ and $LCN2^{-/-}$ mice were examined at 2 days after cortical stab wound injury (*B*). RNA was isolated from the injury site in the cortex and subjected to real time PCR. The injury-induced CXCL10 expression was completely abrogated in $LCN2^{-/-}$ brain as compared with $LCN2^{+/+}$ littermates. GAPDH was used as a control in the real time PCR. The results are the means ± S.D. ($n = 3$). *, $p < 0.05$ compared with uninjured $LCN2^{+/+}$ mice; **, $p < 0.05$ compared with injured $LCN2^{+/+}$ mice; #, $p < 0.05$ compared with uninjured $LCN2^{-/-}$ mice.

immunohistochemical studies. The stab wound injury increased the expression of GFAP in cortex at 2 dpi, indicating the astrocyte migration toward the stab injury site (Fig. 8*A*). $LCN2^{-/-}$ mice showed a reduced astrocyte migration in response to cortical stab wound injury, when compared with $LCN2^{+/+}$ mice (Fig. 8*A*). After the stab wound injury, the expression of LCN2 and CXCL10 was also investigated by quantitative real time PCR. The stab wound injury significantly increased the expression of *lcn2* and CXCL10 mRNA at injury site compared with uninjured control mice (Fig. 8*B*). The expression of *lcn2* and CXCL10 was negligible in the cortex of $LCN2^{-/-}$ mice after the focal injury in the cortex (Fig. 8*B*). These results further support the important role of LCN2 in the regulation of CXCL10 expression. In the next set of experiments, $LCN2^{+/+}$ and $LCN2^{-/-}$ received intracortical or intracerebroventricular injection of LPS. The animals were then perfused, and brain tissue was prepared for immunohistochemical studies. LCN2 expression was found in the cortex and hippocampus, and the expression was completely absent in $LCN2^{-/-}$ mice as anticipated (Fig. 9, *A* and *B*), a finding that underscores the appropriateness of the polyclonal anti-LCN2 antibody for the *in vivo* immunohistochemical studies. The injection of LPS noticeably increased the expression of LCN2 and GFAP in the cortex or hippocampus of $LCN2^{+/+}$ mice when compared with saline-injected controls at 2 dpi (Fig. 9, *A* and *B*). After LPS injection, the number of GFAP-positive astrocytes in $LCN2^{-/-}$ mice was significantly lower than that found in their $LCN2^{+/+}$ littermates (Fig. 9, *A* and *B*). We also evaluated mRNA expression of the chemokine CXCL10, which is expressed in response to inflammatory stimulation, by quantitative real time PCR of cortical tissue around the injection site. LPS-induced CXCL10 expression was almost completely abolished in the cortex of $LCN2^{-/-}$ mice compared with $LCN2^{+/+}$ mice at 2 dpi (Fig. 9*A*), indicating a crucial role for LCN2 in the regulation of CXCL10 expression. GFAP mRNA expression showed a similar pattern (Fig. 9*A*). In addition, there was a decrease in both the number and intensity of GFAP-positive cells in the hippocampus of $LCN2^{-/-}$ mice compared with $LCN2^{+/+}$ mice after icv injection of LPS (Fig. 9*B*). $LCN2^{-/-}$ mice displayed very little staining for LCN2 or GFAP, suggesting a reduced astrocyte migration and neuroinflammation in response to LPS injection. No significant difference in GFAP staining was found in the hippocampus of $LCN2^{-/-}$ mice between saline and LPS injection (data not shown). The increase in GFAP immunoreactivity was mainly detected in the hippocampus following icv injection of LPS in both $LCN2^{+/+}$ and $LCN2^{-/-}$ mice. Quantification of the data revealed 55 and 37% decreases in the number of GFAP-positive cells in the cortex and hippocampus of $LCN2^{-/-}$ mice, respectively, when compared with $LCN2^{+/+}$ mice after LPS injection (Fig. 9, *A* and *B*). In $LCN2^{-/-}$ mice, LPS-induced up-regulation of CXCL10 or GFAP mRNA expression in hippocampal tissue was insignificant, consistent with reduced neuroinflammation (Fig. 9*B*). Additionally, double labeling using antibodies against GFAP and LCN2 in hippocampus of the $LCN2^{+/+}$ mice after icv injection of LPS indicated that LCN2 is expressed in the majority of astrocytes (Fig. 9*C*). Taken together, these results indicate that inflammation or injury-triggered astrocyte migration and GFAP/CXCL10 expression are significantly decreased in

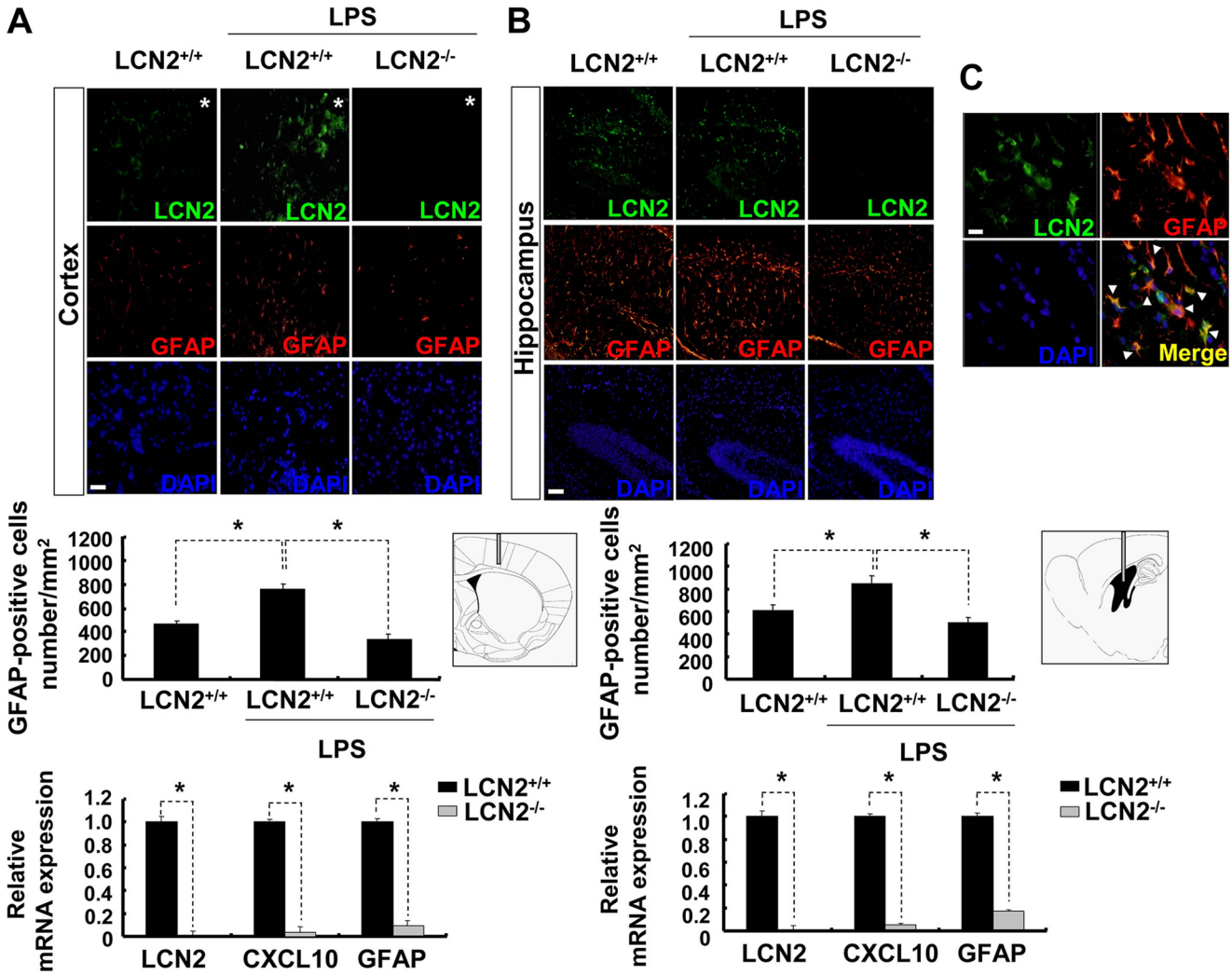

FIGURE 9. **Essential role of LCN2 in reactive astrocytosis and CXCL10 induction in LPS-induced mouse neuroinflammation models.** $LCN2^{+/+}$ or $LCN2^{-/-}$ were injected with LPS intracortically (*A*) or icv (*B*). After 2 dpi, the mice were sacrificed, and cryosections were immunostained with antibodies against LCN2 (*green*, *upper*) or GFAP (*red*, *middle*). The nuclei were counterstained with DAPI (*blue*, *lower*). The *asterisk* indicates the injection site. A significant decrease in both LCN2 and GFAP expression was observed in $LCN2^{-/-}$ mice. The results are one representative of more than three independent experiments. *Scale bars*, 100 μm. Quantification of the GFAP-positive cells was done in the cortex (*A*, *upper graph*) or hippocampus (*B*, *upper graph*). The values are the means ± S.D. from three different animals and five independent sections per animal. The mRNA levels of *lcn2*, CXCL10, and GFAP in $LCN2^{+/+}$ and $LCN2^{-/-}$ mice were examined by real time PCR of cortical tissue around the injection site (*A*, *lower graph*) or hippocampus (*B*, *lower graph*) at 2 days after intracortical or icv injection with LPS, respectively. $LCN2^{-/-}$ mice exhibited markedly lower levels of CXCL10 and GFAP as compared with $LCN2^{+/+}$ littermates. *, $p < 0.05$; compared with wild-type LPS-injected mice ($LCN2^{+/+}$) at the same inflammation model. At 2 days after icv injection of $LCN2^{+/+}$ mice with LPS, hippocampus was immunostained with antibodies against LCN2 (*green*) or GFAP (*red*) (*C*). The nuclei were counterstained with DAPI (*blue*). A merged image is shown in the *lower right panel*. The *arrowheads* indicate colocalization of LCN2 and GFAP (*yellow*). Cell bodies and processes of astrocytes in hippocampus were stained with LCN2 antibody. The results are representative of more than three independent experiments. *Scale bars*, 20 μm.

$LCN2^{-/-}$ mouse brain, supporting the pivotal role of LCN2 in reactive astrocytosis and brain inflammation *in vivo*.

DISCUSSION

In this study, we report that LCN2 up-regulates chemokine expression in the CNS cells and that these chemokines mediate LCN2-induced cell migration. LCN2 has been previously implicated in cell migration in a variety of different tissue types. LCN2 has been associated with an increased migratory activity of breast cancer (5, 57) and other cell types (6, 13, 58), which is consistent with the stimulating role of LCN2 in astrocyte migration, as demonstrated in our previous (18) and current studies. Thus, chemokines seem to mediate the cell migration-promoting activity of LCN2, at least in the CNS.

Chemokines in the brain have been shown to exert neuromodulatory activity and to be involved in the migration of a broad spectrum of cells, including astrocytes, microglia, and neurons (32). For instance, astrocyte migration has been demonstrated, *in vitro*, in response to CCL2, CXCL10, and CXCL12 (30, 31, 59). Although the expression of chemokines is commonly induced by inflammatory cytokines and pathogens (60), less is known about other molecular mediators that induce chemokine expression in the CNS. The expression of chemokines is regulated by many stimulatory and inhibitory factors, such as Toll-like receptor-3, UDP, TGF-β, 17β-estradiol, and HIV-1 glycoprotein 120 in the CNS (19–21, 61–65). Now, our results indicate that chemokine expression is highly up-regulated by LCN2 and that these chemokines promote the migra-

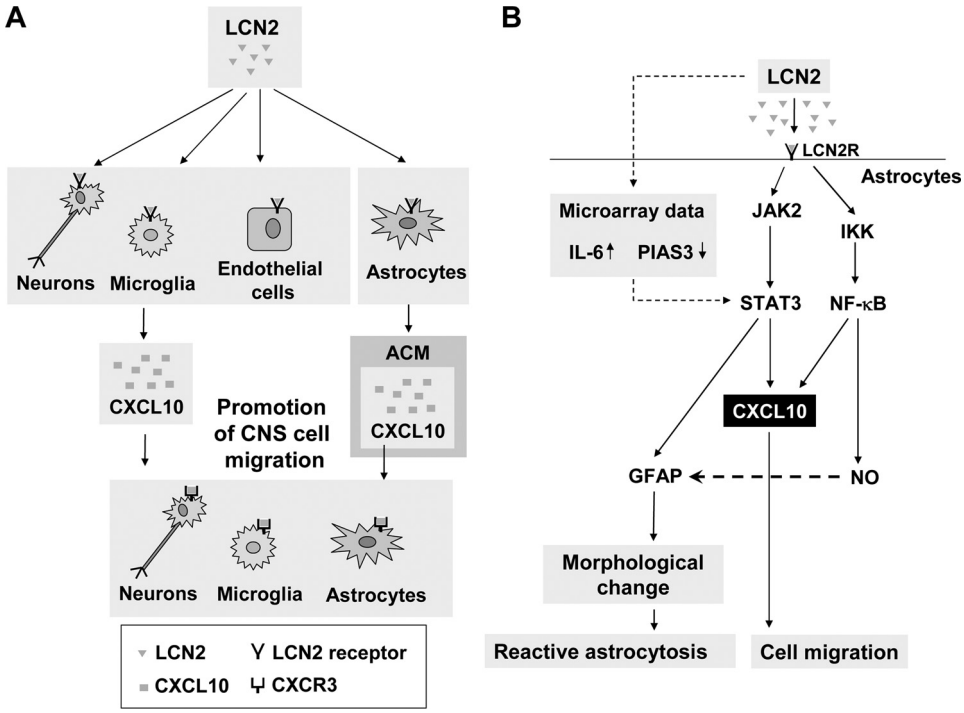

FIGURE 10. **Schematic diagram depicting the promotion of CNS cell migration by LCN2-induced CXCL10 (*A*) and the possible pathway through which LCN2 induces astrocyte migration and morphological changes (*B*).** *A*, LCN2 up-regulates CXCL10 expression in the multiple cell types in the CNS, such as astrocytes, microglia, neurons, and endothelial cells. Astrocyte-derived CXCL10 acts in a paracrine or autocrine manner to promote cell migration in the inflammatory scene. CXCL10 secreted by other cell types may play a similar role. The *lcn2* receptor and CXCL10 receptor (CXCR3) are widely expressed in glia, endothelial cells, and neurons. *B*, LCN2 up-regulates CXCL10 and GFAP expression in reactive astrocytes through JAK2/STAT3 and NF-κB pathways. Although LCN2-up-regulated CXCL10 promotes cell migration, GFAP induction may lead to morphological changes observed in reactive astrocytosis. Based on the microarray analysis, LCN2 induces the up-regulation of IL-6 and down-regulation of PIAS3, thereby facilitating the STAT3 pathway (*dotted line*). NO production, downstream of the NF-κB, may cooperate with the STAT3 pathway to induce GFAP expression. NO has been shown to induce GFAP expression in astrocytes (*bold dotted line*) (54). Moreover, IL-6 previously induced GFAP expression through the STAT3 pathway (96). Other pathways may also participate in astrocyte migration and morphological change under the current conditions.

tion of astrocytes, microglia, and neurons. Although the important role of CXCL10 in LCN2-induced cell migration has been demonstrated in this study, other chemokines and nonchemokines may also participate in LCN2-induced CNS cell migration. Moreover, cross-talk between chemokine and nonchemokine pathways may also be potentially important in controlling brain cell migration. Neuronal guidance molecules such as netrins, ephrins, semaphorins, slits, and the chemokine SDF have been previously implicated in regulating neuronal migration (66–74). The netrin, slit, semaphorin, and ephrin pathways are versatile, because these guidance cues have been implicated in a wide variety of axon guidance or targeting events. The functions of these guidance molecules are not restricted to axon migrations. Netrins and slits influence neuronal as well as mesodermal cell migrations (75–77); semaphorins mediate bone and heart morphogenesis (78); and ephrins direct neural crest migration and angiogenesis (79). Furthermore, semaphorins and slits affect the growth of retinal ganglion cell axons (80, 81).

We have previously shown that LCN2 plays a central role in reactive astrocytosis. LCN2 induced GFAP expression and cell migration in astrocytes (18). One of the hallmarks of reactive astrocytosis is an increase in the number of astrocytes. A local increase in the cell number may be due to either increased cell proliferation or recruitment of cells. The enhanced expression of chemokines and chemokine receptors has been described under various pathological conditions, such as multiple sclerosis, HIV infection, ischemia, and neoplasm (82–84). Reactive astrocytes express various chemokines and their receptors, which induce cell migration and other cellular reactions that are generally involved in reactive astrocytosis. Thus, chemokines may mediate the cell migration-promoting activity of LCN2 during reactive astrocytosis. Reactive astrocytosis is also accompanied by morphological changes. The involvement of LCN2 in the phenotypic change of cell morphology has been previously reported. LCN2 induced a process extension in astrocytes (18). LCN2 was an endogenous epithelial inducer (7) and stimulated the epithelial phenotype of transformed cells (85, 86). LCN2 also promoted tubulogenesis by regulating epithelial morphogenesis (87). LCN2-induced chemokines may participate in the modification of cell morphology. Previously, CCL5/RANTES, one of the inflammatory chemokines secreted by astrocytes, was critical for promoting neurite outgrowth and migration in cortical neurons. Therefore, chemokines secreted by activated astrocytes and other CNS cells may mediate distinct morphological changes in addition to cell migration (Figs. 3–6).

The JAK-STAT signaling pathway is known to be involved in hematopoiesis (88), immune responses (89), cellular homeostasis (90), gliogenesis (91), and reactive astrocytosis (53, 92). In the CNS, STAT3 is expressed by astrocytes, neurons, and other glial cell types (93), and the activation of STAT3 by phosphorylation markedly increases after CNS insults (94, 95). Here, we showed that the LCN2 induction of CXCL10 expression in

astrocytes was partly mediated by the JAK2/STAT3 pathway, which was in accordance with a microarray analysis showing the down-regulation of the PIAS3 by LCN2 (Fig. 1*A* and Table 2). Previously, cAMP-induced autocrine IL-6 enhanced the GFAP expression through STAT3. IL-6 was important for STAT3 activation and subsequent GFAP expression (96). Consistently, in this study, LCN2 also increased IL-6 expression in astrocytes (Fig. 1, *A* and *E*, and Table 2). The JAK2/STAT3 pathway was also involved in LCN2-induced GFAP expression. Thus, the JAK2/STAT3 signaling pathway appears to play a pivotal role in the LCN2 action in astrocytes. Our results indicated NF-κB as an additional signaling pathway that regulates the LCN2 actions (Fig. 7).

The critical role of LCN2 in CNS cell migration and reactive astrocytosis *in vivo* was demonstrated in mouse brain injury or inflammation models. Injection of LPS into specific regions of rodent brain results in the activation of glial cells and inflammatory responses typically found in neuroinflammatory and neurodegenerative diseases (97–99). The LPS injection model has been extensively used to analyze the cellular and molecular mechanisms underlying inflammatory responses in the CNS (99, 100). In the current study, either cortical/icv injection of LPS or stab wound insult was performed to induce brain inflammation or injury. The injection of LPS or stab wound injury increased the expression of GFAP and CXCL10 in the brain. Importantly, the induction of GFAP and CXCL10 was markedly reduced in the brain of $LCN2^{-/-}$ mice, suggesting that GFAP and CXCL10 expression is regulated by LCN2. The LPS-triggered expression of LCN2 and GFAP was colocalized, which was consistent with previous studies demonstrating that LCN2 was induced in primary astrocyte cultures under inflammatory conditions *in vitro* (18).

In summary, we present evidence that inflammatory chemokines are up-regulated in LCN2-treated astrocytes, microglia, endothelial cells, and neuronal cells. Chemokines, CXCL10 in particular, secreted from LCN2-treated astrocytes promoted the migration of microglia and neurons, as well as astrocytes themselves (see Fig. 10 for schematic diagram). The JAK2/STAT3 and IKK/NF-κB pathways were involved in the LCN2 induction of CXCL10 secretion and possibly other phenotypic changes associated with reactive astrocytosis. More importantly, mice lacking LCN2 showed an impaired astrocyte migration and a reduced expression of GFAP and CXCL10 following LPS exposure or stab wound injury. These results clearly establish an essential role for LCN2 as a protein required for the reactive astrocytosis and cell migration in the CNS. Thus, we propose that LCN2 is a chemokine inducer in the CNS and may accelerate cell migration under inflammatory conditions in an autocrine or paracrine manner. Lastly, our data suggest that LCN2 could be targeted to therapeutically modulate glial responses in various neuroinflammatory disease conditions.

Acknowledgment—We thank Dr. Shizuo Akira (Osaka University, Osaka, Japan) for generously providing the LCN2-deficient mice.

REFERENCES

1. Devireddy, L. R., Gazin, C., Zhu, X., and Green, M. R. (2005) *Cell* **123,** 1293–1305
2. Nelson, A. M., Zhao, W., Gilliland, K. L., Zaenglein, A. L., Liu, W., and Thiboutot, D. M. (2008) *J. Clin. Invest.* **118,** 1468–1478
3. Tong, Z., Wu, X., Ovcharenko, D., Zhu, J., Chen, C. S., and Kehrer, J. P. (2005) *Biochem. J.* **391,** 441–448
4. Kehrer, J. P. (2010) *Cell Biol. Toxicol.* **26,** 83–89
5. Yang, J., Bielenberg, D. R., Rodig, S. J., Doiron, R., Clifton, M. C., Kung, A. L., Strong, R. K., Zurakowski, D., and Moses, M. A. (2009) *Proc. Natl. Acad. Sci. U.S.A.* **106,** 3913–3918
6. Bauer, M., Eickhoff, J. C., Gould, M. N., Mundhenke, C., Maass, N., and Friedl, A. (2008) *Breast Cancer Res. Treat.* **108,** 389–397
7. Yang, J., Goetz, D., Li, J. Y., Wang, W., Mori, K., Setlik, D., Du, T., Erdjument-Bromage, H., Tempst, P., Strong, R., and Barasch, J. (2002) *Mol. Cell* **10,** 1045–1056
8. Bolignano, D., Donato, V., Coppolino, G., Campo, S., Buemi, A., Lacquaniti, A., and Buemi, M. (2008) *Am. J. Kidney Dis.* **52,** 595–605
9. Flo, T. H., Smith, K. D., Sato, S., Rodriguez, D. J., Holmes, M. A., Strong, R. K., Akira, S., and Aderem, A. (2004) *Nature* **432,** 917–921
10. Mori, K., Lee, H. T., Rapoport, D., Drexler, I. R., Foster, K., Yang, J., Schmidt-Ott, K. M., Chen, X., Li, J. Y., Weiss, S., Mishra, J., Cheema, F. H., Markowitz, G., Suganami, T., Sawai, K., Mukoyama, M., Kunis, C., D'Agati, V., Devarajan, P., and Barasch, J. (2005) *J. Clin. Invest.* **115,** 610–621
11. Liu, Q., and Nilsen-Hamilton, M. (1995) *J. Biol. Chem.* **270,** 22565–22570
12. Yan, Q. W., Yang, Q., Mody, N., Graham, T. E., Hsu, C. H., Xu, Z., Houstis, N. E., Kahn, B. B., and Rosen, E. D. (2007) *Diabetes* **56,** 2533–2540
13. Playford, R. J., Belo, A., Poulsom, R., Fitzgerald, A. J., Harris, K., Pawluczyk, I., Ryon, J., Darby, T., Nilsen-Hamilton, M., Ghosh, S., and Marchbank, T. (2006) *Gastroenterology* **131,** 809–817
14. Lin, H. H., Liao, C. J., Lee, Y. C., Hu, K. H., Meng, H. W., and Chu, S. T. (2011) *Int. J. Biol. Sci.* **7,** 74–86
15. Lim, R., Ahmed, N., Borregaard, N., Riley, C., Wafai, R., Thompson, E. W., Quinn, M. A., and Rice, G. E. (2007) *Int. J. Cancer* **120,** 2426–2434
16. Tong, Z., Kunnumakkara, A. B., Wang, H., Matsuo, Y., Diagaradjane, P., Harikumar, K. B., Ramachandran, V., Sung, B., Chakraborty, A., Bresalier, R. S., Logsdon, C., Aggarwal, B. B., Krishnan, S., and Guha, S. (2008) *Cancer Res.* **68,** 6100–6108
17. Lee, S., Lee, J., Kim, S., Park, J. Y., Lee, W. H., Mori, K., Kim, S. H., Kim, I. K., and Suk, K. (2007) *J. Immunol.* **179,** 3231–3241
18. Lee, S., Park, J. Y., Lee, W. H., Kim, H., Park, H. C., Mori, K., and Suk, K. (2009) *J. Neurosci.* **29,** 234–249
19. Charo, I. F., and Ransohoff, R. M. (2006) *N. Engl. J. Med.* **354,** 610–621
20. Ubogu, E. E., Cossoy, M. B., and Ransohoff, R. M. (2006) *Trends Pharmacol. Sci.* **27,** 48–55
21. Bertollini, C., Ragozzino, D., Gross, C., Limatola, C., and Eusebi, F. (2006) *Neuropharmacology* **51,** 816–821
22. Rostène, W., Kitabgi, P., and Parsadaniantz, S. M. (2007) *Nat. Rev. Neurosci.* **8,** 895–903
23. Sallusto, F., Mackay, C. R., and Lanzavecchia, A. (2000) *Annu. Rev. Immunol.* **18,** 593–620
24. Vanguri, P. (1995) *J. Neuroimmunol.* **56,** 35–43
25. Luster, A. D., Unkeless, J. C., and Ravetch, J. V. (1985) *Nature* **315,** 672–676
26. Majumder, S., Zhou, L. Z., Chaturvedi, P., Babcock, G., Aras, S., and Ransohoff, R. M. (1998) *J. Neurosci. Res.* **54,** 169–180
27. Hesselgesser, J., and Horuk, R. (1999) *J. Neurovirol.* **5,** 13–26
28. Sun, D., Hu, X., Liu, X., Whitaker, J. N., and Walker, W. S. (1997) *J. Neurosci. Res.* **48,** 192–200
29. Fisher, S. N., Vanguri, P., Shin, H. S., and Shin, M. L. (1995) *Brain Behav. Immun.* **9,** 331–344
30. Biber, K., Dijkstra, I., Trebst, C., De Groot, C. J., Ransohoff, R. M., and Boddeke, H. W. (2002) *Neuroscience* **112,** 487–497
31. Odemis, V., Moepps, B., Gierschik, P., and Engele, J. (2002) *J. Biol. Chem.* **277,** 39801–39808
32. Ambrosini, E., and Aloisi, F. (2004) *Neurochem. Res.* **29,** 1017–1038
33. Montesano, R., Pepper, M. S., Möhle-Steinlein, U., Risau, W., Wagner, E. F., and Orci, L. (1990) *Cell* **62,** 435–445
34. Enokido, Y., Akaneya, Y., Niinobe, M., Mikoshiba, K., and Hatanaka, H.

(1992) *Brain Res.* **599,** 261–271
35. Araki, W., Yuasa, K., Takeda, S., Shirotani, K., Takahashi, K., and Tabira, T. (2000) *Ann. N.Y. Acad. Sci.* **920,** 241–244
36. Livak, K. J., and Schmittgen, T. D. (2001) *Methods* **25,** 402–408
37. Cheeran, M. C., Hu, S., Sheng, W. S., Peterson, P. K., and Lokensgard, J. R. (2003) *J. Virol.* **77,** 4502–4515
38. Neptune, E. R., and Bourne, H. R. (1997) *Proc. Natl. Acad. Sci. U.S.A.* **94,** 14489–14494
39. Liang, C. C., Park, A. Y., and Guan, J. L. (2007) *Nat. Protoc.* **2,** 329–333
40. Bassi, R., Giussani, P., Anelli, V., Colleoni, T., Pedrazzi, M., Patrone, M., Viani, P., Sparatore, B., Melloni, E., and Riboni, L. (2008) *J. Neurooncol.* **87,** 23–33
41. Wilhelmsson, U., Li, L., Pekna, M., Berthold, C. H., Blom, S., Eliasson, C., Renner, O., Bushong, E., Ellisman, M., Morgan, T. E., and Pekny, M. (2004) *J. Neurosci.* **24,** 5016–5021
42. Borán, M. S., and García, A. (2007) *J. Neurochem.* **102,** 216–230
43. Chou, S. Y., Weng, J. Y., Lai, H. L., Liao, F., Sun, S. H., Tu, P. H., Dickson, D. W., and Chern, Y. (2008) *J. Neurosci.* **28,** 3277–3290
44. Kalla, R., Bohatschek, M., Kloss, C. U., Krol, J., Von Maltzan, X., and Raivich, G. (2003) *Glia* **41,** 50–63
45. Hwang, J., Zheng, L. T., Ock, J., Lee, M. G., and Suk, K. (2008) *Int. Immunopharmacol.* **8,** 1686–1694
46. Nairz, M., Theurl, I., Schroll, A., Theurl, M., Fritsche, G., Lindner, E., Seifert, M., Crouch, M. L., Hantke, K., Akira, S., Fang, F. C., and Weiss, G. (2009) *Blood* **114,** 3642–3651
47. Chung, R. S., Leung, Y. K., Butler, C. W., Chen, Y., Eaton, E. D., Pankhurst, M. W., West, A. K., and Guillemin, G. J. (2009) *Neurotox. Res.* **15,** 381–389
48. Andersson, P. B., Perry, V. H., and Gordon, S. (1992) *Neuroscience* **48,** 169–186
49. Schmidt-Ott, K. M., Mori, K., Kalandadze, A., Li, J. Y., Paragas, N., Nicholas, T., Devarajan, P., and Barasch, J. (2006) *Curr. Opin. Nephrol. Hypertens.* **15,** 442–449
50. Hvidberg, V., Jacobsen, C., Strong, R. K., Cowland, J. B., Moestrup, S. K., and Borregaard, N. (2005) *FEBS Lett.* **579,** 773–777
51. Omari, K. M., John, G. R., Sealfon, S. C., and Raine, C. S. (2005) *Brain* **128,** 1003–1015
52. Chung, C. D., Liao, J., Liu, B., Rao, X., Jay, P., Berta, P., and Shuai, K. (1997) *Science* **278,** 1803–1805
53. Herrmann, J. E., Imura, T., Song, B., Qi, J., Ao, Y., Nguyen, T. K., Korsak, R. A., Takeda, K., Akira, S., and Sofroniew, M. V. (2008) *J. Neurosci.* **28,** 7231–7243
54. Brahmachari, S., Fung, Y. K., and Pahan, K. (2006) *J. Neurosci.* **26,** 4930–4939
55. Sunil, V. R., Patel, K. J., Nilsen-Hamilton, M., Heck, D. E., Laskin, J. D., and Laskin, D. L. (2007) *Exp. Mol. Pathol.* **83,** 177–187
56. Marques, F., Rodrigues, A. J., Sousa, J. C., Coppola, G., Geschwind, D. H., Sousa, N., Correia-Neves, M., and Palha, J. A. (2008) *J. Cereb. Blood Flow Metab.* **28,** 450–455
57. Shi, H., Gu, Y., Yang, J., Xu, L., Mi, W., and Yu, W. (2008) *J. Exp. Clin. Cancer Res.* **27,** 83
58. Zhang, H., Xu, L., Xiao, D., Xie, J., Zeng, H., Wang, Z., Zhang, X., Niu, Y., Shen, Z., Shen, J., Wu, X., and Li, E. (2007) *J. Clin. Pathol.* **60,** 555–561
59. Andjelkovic, A. V., Song, L., Dzenko, K. A., Cong, H., and Pachter, J. S. (2002) *J. Neurosci. Res.* **70,** 219–231
60. Chensue, S. W. (2001) *Clin. Microbiol. Rev.* **14,** 821–835
61. Park, C., Lee, S., Cho, I. H., Lee, H. K., Kim, D., Choi, S. Y., Oh, S. B., Park, K., Kim, J. S., and Lee, S. J. (2006) *Glia* **53,** 248–256
62. Kim, B., Jeong, H. K., Kim, J. H., Lee, S. Y., Jou, I., and Joe, E. H. (2011) *J. Immunol.* **186,** 3701–3709
63. Paglinawan, R., Malipiero, U., Schlapbach, R., Frei, K., Reith, W., and Fontana, A. (2003) *Glia* **44,** 219–231
64. Matejuk, A., Adlard, K., Zamora, A., Silverman, M., Vandenbark, A. A., and Offner, H. (2001) *J. Neurosci. Res.* **65,** 529–542
65. Missé, D., Esteve, P. O., Renneboog, B., Vidal, M., Cerutti, M., St Pierre, Y., Yssel, H., Parmentier, M., and Veas, F. (2001) *Blood* **98,** 541–547
66. Colamarino, S. A., and Tessier-Lavigne, M. (1995) *Annu. Rev. Neurosci.* **18,** 497–529
67. Hu, H., and Rutishauser, U. (1996) *Neuron* **16,** 933–940
68. Flanagan, J. G., and Vanderhaeghen, P. (1998) *Annu. Rev. Neurosci.* **21,** 309–345
69. Wu, W., Wong, K., Chen, J., Jiang, Z., Dupuis, S., Wu, J. Y., and Rao, Y. (1999) *Nature* **400,** 331–336
70. Zhu, Y., Li, H., Zhou, L., Wu, J. Y., and Rao, Y. (1999) *Neuron* **23,** 473–485
71. Raper, J. A. (2000) *Curr. Opin. Neurobiol.* **10,** 88–94
72. Klein, R. S., Rubin, J. B., Gibson, H. D., DeHaan, E. N., Alvarez-Hernandez, X., Segal, R. A., and Luster, A. D. (2001) *Development* **128,** 1971–1981
73. Guan, K. L., and Rao, Y. (2003) *Nat. Rev. Neurosci.* **4,** 941–956
74. Nguyen-Ba-Charvet, K. T., Picard-Riera, N., Tessier-Lavigne, M., Baron-Van Evercooren, A., Sotelo, C., and Chédotal, A. (2004) *J. Neurosci.* **24,** 1497–1506
75. Hedgecock, E. M., Culotti, J. G., and Hall, D. H. (1990) *Neuron* **4,** 61–85
76. Ackerman, S. L., Kozak, L. P., Przyborski, S. A., Rund, L. A., Boyer, B. B., and Knowles, B. B. (1997) *Nature* **386,** 838–842
77. Kramer, S. G., Kidd, T., Simpson, J. H., and Goodman, C. S. (2001) *Science* **292,** 737–740
78. Behar, O., Golden, J. A., Mashimo, H., Schoen, F. J., and Fishman, M. C. (1996) *Nature* **383,** 525–528
79. Wilkinson, D. G. (2001) *Nat. Rev. Neurosci.* **2,** 155–164
80. Erskine, L., Williams, S. E., Brose, K., Kidd, T., Rachel, R. A., Goodman, C. S., Tessier-Lavigne, M., and Mason, C. A. (2000) *J. Neurosci.* **20,** 4975–4982
81. Niclou, S. P., Jia, L., and Raper, J. A. (2000) *J. Neurosci.* **20,** 4962–4974
82. Goldberg, S. H., van der Meer, P., Hesselgesser, J., Jaffer, S., Kolson, D. L., Albright, A. V., González-Scarano, F., and Lavi, E. (2001) *Neuropathol. Appl. Neurobiol.* **27,** 127–138
83. Simpson, J., Rezaie, P., Newcombe, J., Cuzner, M. L., Male, D., and Woodroofe, M. N. (2000) *J. Neuroimmunol.* **108,** 192–200
84. Tanuma, N., Sakuma, H., Sasaki, A., and Matsumoto, Y. (2006) *Acta Neuropathol.* **112,** 195–204
85. Lee, H. J., Lee, E. K., Lee, K. J., Hong, S. W., Yoon, Y., and Kim, J. S. (2006) *Int. J. Cancer* **118,** 2490–2497
86. Hanai, J., Mammoto, T., Seth, P., Mori, K., Karumanchi, S. A., Barasch, J., and Sukhatme, V. P. (2005) *J. Biol. Chem.* **280,** 13641–13647
87. Gwira, J. A., Wei, F., Ishibe, S., Ueland, J. M., Barasch, J., and Cantley, L. G. (2005) *J. Biol. Chem.* **280,** 7875–7882
88. Kisseleva, T., Bhattacharya, S., Braunstein, J., and Schindler, C. W. (2002) *Gene* **285,** 1–24
89. Ivashkiv, L. B. (2000) *Rev. Immunogenet.* **2,** 220–230
90. Schindler, C. W. (2002) *J. Clin. Invest.* **109,** 1133–1137
91. Sauvageot, C. M., and Stiles, C. D. (2002) *Curr. Opin. Neurobiol.* **12,** 244–249
92. Na, Y. J., Jin, J. K., Kim, J. I., Choi, E. K., Carp, R. I., and Kim, Y. S. (2007) *J. Neurochem.* **103,** 637–649
93. Cattaneo, E., Conti, L., and De-Fraja, C. (1999) *Trends Neurosci.* **22,** 365–369
94. Sriram, K., Benkovic, S. A., Hebert, M. A., Miller, D. B., and O'Callaghan, J. P. (2004) *J. Biol. Chem.* **279,** 19936–19947
95. Yamauchi, K., Osuka, K., Takayasu, M., Usuda, N., Nakazawa, A., Nakahara, N., Yoshida, M., Aoshima, C., Hara, M., and Yoshida, J. (2006) *J. Neurochem.* **96,** 1060–1070
96. Takanaga, H., Yoshitake, T., Hara, S., Yamasaki, C., and Kunimoto, M. (2004) *J. Biol. Chem.* **279,** 15441–15447
97. Kitazawa, M., Oddo, S., Yamasaki, T. R., Green, K. N., and LaFerla, F. M. (2005) *J. Neurosci.* **25,** 8843–8853
98. Czapski, G. A., Cakala, M., Chalimoniuk, M., Gajkowska, B., and Strosznajder, J. B. (2007) *J. Neurosci. Res.* **85,** 1694–1703
99. Qin, L., Wu, X., Block, M. L., Liu, Y., Breese, G. R., Hong, J. S., Knapp, D. J., and Crews, F. T. (2007) *Glia* **55,** 453–462
100. Cunningham, C., Wilcockson, D. C., Campion, S., Lunnon, K., and Perry, V. H. (2005) *J. Neurosci.* **25,** 9275–9284